

**DEVELOPMENT OF A SUBCORTICAL EMPHASIZED
PHYSICAL HUMAN HEAD MODEL FOR EVALUATION OF
DEEP BRAIN SOURCE CONTRIBUTION TO SCALP EEG**

YE YAN

(B.Eng.(Hons.), NUS)

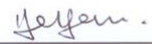
A THESIS SUBMITTED
FOR THE DEGREE OF DOCTOR OF PHILOSOPHY
DEPARTMENT OF MECHANICAL ENGINEERING
NATIONAL UNIVERSITY OF SINGAPORE

2014

DECLARATION

I hereby declare that this thesis is my original work and it has been written by me in its entirety. I have duly acknowledged all the sources of information which have been used in the thesis.

This thesis has also not been submitted for any degree in any university previously.



Ye Yan

27 September 2014

PUBLICATIONS

Journal Paper

- [1] **Yan Ye**, Wu Chun Ng, Xiaoping Li*, Study of the ionic conductivity of a gelatin-NaCl electrolyte, *International Journal of Computer Application in Technology*, 2012, accepted.
- [2] **Yan Ye**, Xiaoping Li*, Tiecheng Wu, Zhe Li and Wenwen Xie. Material and physical model for evaluation of deep brain activity contribution to EEG recordings, *Functional Materials Letters*, December 2014, published.
- [3] **Yan Ye**, Xiaoping Li* and Wenwen Xie, Material and physical model for source localization studies of cortical and deep brain activity using LORETA method, *Material Technology – High Performance Materials*, 2014, September, submitted.
- [4] Z. Li, D.G. Yang, W.D. Hao, S. Wu, **Y. Ye**, Z.D. Chen and X. P. Li, Ultrasound vibration assisted micro hole forming on skull, *Part B: Journal of Engineering Manufacture*, September 2014, submitted.

Conference Paper

- [1] **Yan Ye**, Wei Qian Ser, Tiecheng Wu, Zhe Li and Xiaoping Li*, Material and physical model for evaluation of cortical and deep brain activity contribution to scalp EEG recordings, *6th International Symposium on Functional Materials (ISFM Paper 104)*, August 2014.
- [2] **Yan Ye**, Zhe Li, Tiecheng Wu and Xiaoping Li*, Material and physical model for source localization studies of cortical and deep brain activity using LORETA method, *6th International Symposium on Functional Materials (ISFM Paper 183)*, August 2014.
- [3] Zhe Li, Khoon Siong Ng, **Yan Ye** and Xiaoping Li, How thin can a deep brain stimulation lead be? , *Neurology*, 2014, Vol 82 (10), Supplement P7, 041.
- [4] Zhe Li, Khoon Siong Ng, **Yan Ye** and Xiaoping Li, Ultrasound-assisted sub-millimeter burr hole formation on the skull, *11th Asia-Pacific Conference on Materials Processing*, Auckland, New Zealand, 2014.
- [5] Jie Fan, Tiecheng Wu, **Yan Ye**, Ha Duc Bui, Xiaoping Li*, A magnetic field projector for deep brain modulation, *6th International IEEE EMBS Conference on Neural Engineering*, November 2013.
- [6] **Yan Ye**, Yue Wang, Jie Fan, Xiaoping Li*, Evaluation of a human head phantom system for visual event-related potential studies, *International Forum on Systems and Mechatronics (IFSM Paper 10)*, July 2013.

- [7] **Yan Ye**, Yan Liang Tan, Xiaoping Li*, Study of the ionic conductivity of a gelatin-NaCl volume conductor, *International Conference of Young Researchers on Advanced Materials (ICYRAM)*, ICYRAM12-A-01224(EM4), July 2012.
- [8] **Yan Ye**, Wu Chun Ng, Xiaoping Li*, Study of the Ionic Conductivity of a gelatin-NaCl electrolyte”, *International Forum on Functional Materials (IFFM) Proceedings*, IFFM0625, 2011.
- [9] Wu Chun Ng, Wei Long Khoa, **Yan Ye**, Yao Jun Fang and Xiaoping Li, In-vivo measurement of the effect of compression loading on the human skin impedance, *The 3rd International Forum on Systems and Mechatronics (IFSM)*, IFSM040, September 2010.

Conference Presentation Award

- [1] Best Poster Award:
The 6th International Symposium on Functional Materials (ISFM Paper 104) August 2014.
- [2] Best Session Paper Award:
The 3rd International Forum on Systems and Mechatronics (IFSM 2010): functional and integration of mechatronics sensors/devices/systems.

ACKNOWLEDGEMENTS

This thesis is the end of my journey in pursuing the PhD degree. Along the journey, I was encouraged and helped by many people. Without them, the thesis completion is not possible.

First and foremost, I would like to express my sincere appreciation and thanks to my PhD supervisor, Professor Li Xiaoping, for always being supportive during the past four years. He has provided me with insightful discussions about my research and also provided important guidance for my research direction whenever I was lost.

I would like to thank the former and present members in our laboratory, Dr. Shen Kaiquan, Dr. Ning Ning, Dr. Shao Shiyun, Dr. Ng Wu Chun, Dr. Fan Jie, Dr. Yu Ke, Dr. Khoa Wei Long Geoffrey, Dr. Bui Ha Duc, Ms. Wang Yue, Mr. Wu Tiecheng, Mr. Li Zhe, Mr. Ng Khoon Siong and Mr. Rohit Tyagi for their encouragement and help during my PhD journey.

I also thank my final year project students who made contribution to part of the experimental work.

I especially acknowledge Dr. Ma Sha, Mr. Tan Choon Huat and his colleagues for their technical support.

I would like to thank NUS for the research scholarship given to me.

Last but not least, I gratefully thank the most important persons in my life, my parents, my husband, my five-month old baby boy and my parents-in-law. My parents and parents-in-law sacrificed their time to help me take care of baby. My husband and son have always been mentally supportive. I love you all.

TABLE OF CONTENTS

PUBLICATIONS.....	i
ACKNOWLEDGEMENTS.....	iii
TABLE OF CONTENTS.....	iv
SUMMARY.....	vii
LIST OF TABLES.....	ix
LIST OF FIGURES.....	x
LIST OF ABBREVIATIONS AND ACRONYMS.....	xiii
 CHAPTER 1.....	 1
Introduction.....	1
1.1 Motivation.....	1
1.2 Research Objectives.....	3
1.3 Thesis Organization.....	4
CHAPTER 2.....	6
Literature Review.....	6
2.1 Brain Activity Measurement.....	6
2.1.1 Electroencephalography method.....	6
2.1.2 Local field potential method.....	7
2.2 Brain Source Localization.....	9
2.3 Existing Head Models.....	11
2.4 Electrical Properties of Brain, Skull and Scalp.....	14
2.5 Concluding Remarks.....	16
CHAPTER 3.....	17
General Experiment Methods.....	17
3.1 Materials of the Physical Head Model.....	17
3.1.1 Sample preparation of the artificial brain.....	17
3.1.2 Sample preparation of the artificial skull.....	18
3.1.3 Sample preparation of the artificial scalp.....	19
3.2 Electrical Property Measurement.....	21
3.3 The Physical Head Model.....	22

3.4 Electroencephalography Measurement	24
3.5 Low Resolution Brain Electromagnetic Tomography	25
CHAPTER 4	26
Electrical Characteristic Study of the Artificial Brain Material	26
4.1 Introduction	26
4.2 Materials and Methods	28
4.2.1 Gelatin-NaCl electrolytes	28
4.2.2 Impedance spectroscopy measurement	30
4.3 Results and Discussion.....	31
4.3.1 Impedance spectroscopy measurement	31
4.3.2 Temperature dependence of ionic conductivity.....	32
4.4 Empirical Model.....	35
4.5 Concluding Remarks	38
CHAPTER 5	39
Evaluation of the Performance of A Head Phantom System for Event-Related Potential Studies.....	39
5.1 Introduction	39
5.2 Materials and Methods	41
5.2.1 Realistic human head phantom.....	42
5.2.2 Dipolar sources and ERP recordings	46
5.2.3 Forward analysis.....	48
5. 3 Results and Discussion.....	49
5.3.1 Forward matrix analysis	49
5.3.2 Scalp potential map comparison.....	50
5.4 Concluding Remarks	53
CHAPTER 6	55
Evaluation of Deep Brain Activity Contributing to EEG	55
6.1 Introduction	55
6.2 Materials and Methods	56
6.2.1 Experiment.....	56
6.2.2 Signal processing.....	59
6.2.3 Simulation.....	61
6.3 Results and Discussion.....	62
6.3.1 Comparison between experiment and simulation results	62

6.3.2 Overall experiment results	63
6.3.3 Relationship between surface potential and the depth of dipole	65
6.3.4 Linearity check	66
6.4 Concluding Remarks	66
CHAPTER 7	68
Evaluation of the Performance of LORETA Method Utilized for Deep Brain Source Localization	68
7.1 Introduction	68
7.2 Materials and Methods	69
7.2.1 Construction of the physical head model	69
7.2.2 Electrical property of the head model.....	73
7.2.3 EEG acquisition and source localization	75
7.3 Results and Discussion.....	77
7.3.1 EEG results	77
7.3.2 Source localization results	84
7.4 Concluding Remarks	87
CHAPTER 8	89
Conclusions and Recommendations for Future Work	89
8.1 Conclusions	89
8.2 Recommendations for Future Work	93
Bibliography	94

SUMMARY

The objective of this research is to develop a subcortical emphasized physical human head model for evaluation of deep brain source contribution to scalp EEG recordings. To our knowledge, this model is the world's first physical head model designed for subcortical and deep brain source localization studies. In recent years, electroencephalography (EEG) technique has been extensively utilized in clinical and research settings for brain disorder related disease monitoring and cognitive science studies. Quantifying EEG rhythms through low resolution brain electromagnetic tomography (LORETA) analysis could further provide important biomarkers to determine the underlying neuronal activities in the brain. Although LORETA method has been applied in many cognitive processing and brain disorder diagnosis studies, the performance of LORETA method applied for deep brain source localization has not been studied before. However, research on subcortical and deep brain region is important for understanding memory, emotion and consciousness. In order to assist the evaluation, the world's first subcortical emphasized physical head model was developed in this research. Through a series of preparation studies including investigation on the material electrical property and evaluation of the performance of utilizing the head model for EEG studies, the subcortical emphasized physical head model was finally developed. The novelty of this head model is attributed to the location design of its artificial neuronal sources. The artificial neuronal sources were distributed not only in the brain cortex, but also in the subcortical region and deep brain. Specifically speaking, three artificial neuronal sources were respectively distributed in corpus callosum, thalamus and hypothalamus in the subcortical region. Besides, two more

artificial neuronal sources were designed to distribute in the brain stem including the midbrain and pons. Results of this research showed that the localization errors of LORETA method were 0.49 mm, 2.9 mm and 16.86 mm for dipoles located at cortical region. The localization errors were 25.24 mm and 20.86 mm at corpus callosum and thalamus in the subcortical region. However, the localization errors were significant at hypothalamus (52.65 mm) and brain stem (67.39 mm and 60.65 mm). In conclusion, this research has shown that LORETA method is capable of localizing subcortical neuronal activities in thalamus and corpus callosum. This finding makes a great contribution to the field of deep brain source localization studies. The conventional invasive way of brain disease monitoring in thalamus and corpus region could be discontinued and instead the non-invasive EEG technique together with LORETA source localization analysis could be applied.

LIST OF TABLES

Table 1 Curve fitting results of a, b, and c.....	36
Table 2 Curve fitting results of γ , α , and β	37
Table 3 Compositions of the artificial brain, skull and scalp (all units are grams).	44
Table 4 Electrode location and the scalp potential amplitude at this electrode site for different dipoles.....	81

LIST OF FIGURES

Figure 1: Experimental setup for preparation of gelatin material.....	18
Figure 2: Flowchart of how to make the skull sample.....	19
Figure 3: Flowchart of how to make the scalp sample.	21
Figure 4: (a) Sample impedance testing fixture and (b) LCR meter for impedance measurement.....	22
Figure 5: Assembly of the brain master pattern and the aluminium mold.....	24
Figure 6: (a) Schematic drawing of the experimental setup and (b) the real experimental setup for impedance spectroscopy measurement under different temperature levels.	29
Figure 7: Circuit diagram for impedance spectroscopy measurement of the gelatin-NaCl electrolyte using digital signal analyzer (dotted box indicates the internal circuitry of the analyzer).....	31
Figure 8: Ionic Conductivity of gelatin-NaCl is linearly proportional to temperature (100 - 800 Hz with 0.09g/80ml NaCl).....	33
Figure 9: Ionic Conductivity of gelatin-NaCl as a function of frequency (25-50°C with 0.02g/80ml NaCl).	33
Figure 10: Ionic Conductivity of gelatin-NaCl as a function of frequency (25-50°C with 0.09g/80ml NaCl).	34
Figure 11: Ionic Conductivity of gelatin-NaCl as a function of frequency (25-50°C with 0.5g/80ml NaCl).	34
Figure 12: Ionic Conductivity of gelatin-NaCl as a function of frequency (25-50°C with 0.9g/80ml NaCl).	35
Figure 13: Curve fitting lines (dotted lines) versus experimental data (25-50 °C, 10-800Hz with 0.09g/80ml NaCl).	37
Figure 14: The human head phantom system.	41
Figure 15: Assembly of the three-dimensional design of the head model.....	43
Figure 16: Averaged electrical conductivities of the artificial brain, skull and scalp materials. Red error bars indicated the standard deviations.	45
Figure 17: The final brain prototype.....	46
Figure 18: The original dipolar source waveform.	48
Figure 19: Forward model matrix shows the EEG electrode signal (normalized amplitudes) generated by input sinusoidal waveform (10 Hz, 5 V peak-to-peak) at each of the antenna locations in the head model.....	50

Figure 20: Scalp potential maps (a) experimental results, and (b) LORETA averaged ERP for the 1st peak (left figures) and 2nd peak (right figures). All color bar units: μV	51
Figure 21: Electrical conductivities of the white matter and grey matter for all samples. Sample 1 to sample 6 refer to the dipole source at 10 mm, 24 mm, 38 mm, 52 mm, 66 mm and 80 mm depth. Each column indicates the average value of 6 trials of data measurement and red color error bars give the real data range dispersed from the average value.	57
Figure 22: Prolonged test results of the electrical conductivities of the skull compartment at three electrode sites namely working electrode (WE), ground electrode (GND) and reference electrode (REF). Each column indicates the average value of 5 trials of data measurement and red color error bars give the real data range dispersed from the average value.	58
Figure 23: (a) Experiment setup, (b) dimensions of the coax cable, conductor and screen are used to generate the dipole source, and (c) configuration of the dipole position.	59
Figure 24: Comparison of experiment and simulation results, dipole source signal at 5 V.	63
Figure 25: Colored region shows output signal amplitudes (μV) with $\text{SNR}_{\text{dB}} > 4$ dB recorded at dipole strength of 0.02, 0.05, 0.1, 0.25, 0.5, 0.75, 1, 2, 3, 4 and 5 V peak-to-peak, at dipole depth of 10, 24, 38, 52, 66 and 80 mm. Black region indicates bad signals.	64
Figure 26: Surface potential amplitude decays exponentially as dipole depth increases.	65
Figure 27: Linearity check of the head model.	66
Figure 28: Three-dimensional display of the physical head model with dipoles embedded inside the brain, (a) isometric view, (b) side view, and (c) dipole arrangement from top view.	72
Figure 29: Electrical conductivity of 4 samples of skull material. Each column indicated the average conductivity value of 4 repeated trials and the error bar in red color gave the standard deviation dispersed from the average value. ...	74
Figure 30: Prolonged electrical conductivity test of the scalp layer. Each column indicated the average conductivity value of 18 repeated trials and the error bar in red color gave the standard deviation dispersed from the average value.	75
Figure 31: Experiment setup of the EEG measurement on the physical head model.	76
Figure 32: Two-dimensional displays of the EEG waveforms at each electrode site (dipole D1).	78

Figure 33: (a) Scalp potential map (color bar unit: μV) and (b) EEG power spectrum of dipole source D1.	79
Figure 34: Scalp potential maps (all color bar units: μV) and EEG power spectra of dipole source (a) D2, (b) D3, (c) D4, (d) D5, (e) D6, (f) D7 and (g) D8.....	84
Figure 35: Source localization result of dipole D1. The hotspot region indicated location of the dipole source (X, Y, Z) in Talairach coordinate viewed in the brain atlas.	85
Figure 36: Localization results of the physical head model.	86
Figure 37: Schematic diagram of dipole locations in brain anatomy: D1 at somatosensory cortex, D2 at parietal cortex, D3 at motor cortex, D4 at corpus callosum, D5 at thalamus, D6 at hypothalamus, D7 and D8 at brain stem.. ...	87

LIST OF ABBREVIATIONS AND ACRONYMS

EEG	electroencephalography, electroencephalogram
LORETA	low resolution brain electromagnetic tomography
LFP	local field potential
sLORETA	standardized low resolution brain electromagnetic tomography
gelatin-NaCl	gelatin mixed with sodium chloride
FEA	finite element analysis
NaCl	sodium chloride
3D	three-dimensional
fMRI	functional magnetic resonance imaging
DSA	digital Signal Analyzer
ERP	event-related potential
2D	two-dimensional
WE	working electrode
GND	ground electrode
REF	reference electrode
RP	rapid prototyping
AC	anterior commissure

CHAPTER 1

Introduction

1.1 Motivation

Electroencephalography (EEG) records the underlying brain activities on the scalp. In the process of EEG measurement, multiple electrodes are attached on the scalp and these electrodes are used to capture weak electrical signals generated by the synchronous activation of large population of neurons. The process of EEG measurement does not involve any unsafe treatment to the participants. Owing to its non-invasive, inexpensive and convenient reassessment advantages over the invasive way of brain activity measurement, EEG technique thus has been extensively applied in clinical research and neurophysiological studies. It could be used to monitor brain disorder related disease as a neurophysiological approach. One example of the applications of EEG is to provide assessment and progressive assessment of early stage Parkinson's disease (Han, et al., 2013).

Further, quantifying EEG rhythms could provide important biomarkers for diagnosis of lots of neuropsychiatric and neurological disorders of the nervous system, such as schizophrenia, major depressive disorder, Alzheimer's disease and epilepsy (Li, et al., 2008; Indiradevi, et al., 2008; Dauwels, et al., 2010). One important quantitative EEG analysis technique is low resolution brain electromagnetic tomography (LORETA). This technique is capable of determining the relative activity of regions in the brain based on the EEG recordings captured by surface electrodes along the scalp (Pascual-Marqui,

1999). Unlike EEG is the recording of electrical potential differences on the scalp, LORETA method computes the distribution of the current source density in the brain.

Recently, applications of LORETA source localization method in clinical and research settings are prevalent. These applications include finding the activation of visual cortices, auditory cortices, visual and motor cortices, and face processing cortices (Khateb, et al., 2000; Khateb, et al., 2001; Van, et al., 1998; Gallinat, et al., 2002; Thut, et al., 1999; Pizzagalli, et al., 2000). Besides its applications in aforementioned cognitive processing, LORETA method is also applied to find the activation of epileptic seizures (Worrell, et al., 2000; Seeck, et al., 1998; Lantz, et al., 1997). The empirical validity of LORETA has been well established to estimate neuronal generators in cortical level. However, the performance of LORETA method in subcortical level and deep brain region is not well understood. Knowing that research on subcortical and deep brain region is of paramount importance for understanding memory, emotion and consciousness. It is therefore worth evaluating the performance of LORETA method in subcortical level and deep brain region.

Brain activity measurement and brain source localization necessitates the development of a realistic physical human head model. In this research, the physical head model serves as a medium for the studies of deep brain activity measurement via EEG technique and deep source localization through LORETA analysis.

1.2 Research Objectives

The main objective of this research is to develop the world's first subcortical emphasized physical human head model for evaluation of deep brain source contribution to the scalp EEGs. The novelty of this head model is attributed to the location design of its artificial neuronal sources. The conventional brain source localization studies are only focusing on cortical neuronal activities. In contrast, the artificial neuronal sources designed in this research were distributed not only in the brain cortex, but also in the subcortical region and deep brain.

The main objective is then sub-divided into the following sub-objectives.

- (1) Investigate the electrical characteristics of the artificial brain, skull and scalp materials.
- (2) Evaluate the reliability of using a human head phantom system for EEG studies.
- (3) Evaluate the capability of scalp EEG measurement for observing deep brain activities.
- (4) Evaluate the capability of LORETA source localization method for determining deep brain source locations.

In order to achieve these sub-objectives, the research was divided into four studies. The first study was to characterize the electrical property of the artificial brain material selected in this research. Stability of the electrical conductivity of the artificial skull and scalp layers were shown in the subsequent studies. The second study was to evaluate the reliability of using

the human head phantom system for EEG measurement before using the physical head model for subsequent deep brain activity measurement and deep brain source localization studies. In the third study, a cylindrical head model was developed to determine whether scalp EEG technique was capable of measuring deep brain activities. Finally the fourth study was to evaluate the performance of LORETA method applied in deep brain source localization studies.

1.3 Thesis Organization

There are in total eight chapters in this thesis.

Chapter 1 presents the motivation and objectives of this research, and outlines the content of this thesis.

Chapter 2 presents literature reviews on the techniques of brain activity measurement and LORETA source localization analysis. Besides, existing head model utilized in EEG forward and inverse problem was extensively reviewed. Lastly, electrical properties of the human brain, skull and scalp were reviewed as well.

Chapter 3 introduces the general experiment methods for preparing the sample artificial brain, skull and scalp materials, for electrical conductivity measurement of the sample materials, for EEG experiment and LORETA analysis.

Chapter 4 presents a comprehensive study on the characteristics of the electrical property of the artificial brain material selected in this research.

Chapter 5 evaluates the reliability of using the human head phantom system for EEG studies.

Chapter 6 presents the capability of scalp EEG measurement for observing deep brain activities using a cylindrical head model.

Chapter 7 evaluates the capability of LORETA source localization method for determining deep brain source locations using a subcortical emphasized physical human head model.

Chapter 8 summarizes the findings of the research and gives recommendations for future work.

CHAPTER 2

Literature Review

2.1 Brain Activity Measurement

2.1.1 Electroencephalography method

In 1929, electrical activity of the human brain was first discovered and measured by German physiologist and psychiatrist Hans Berger (Berger, 1929). He recorded the electroencephalogram (EEG) by using surface electrodes placed on the scalp. Later EEG was used to describe clinical absence seizures which began the field of clinical electroencephalography in 1930s.

In clinical applications, EEG is used to diagnose brain disorders such as epilepsy, sleep disorders and depression. This is done by examining the obvious abnormalities in EEG readings due to brain disorders. Besides, EEG technique is also used for research purpose in cognitive science and cognitive psychology to study human emotion and memory recognition.

The extensive application of EEG technique in recent years is owing to its non-invasive nature to measure the underlying neuronal activity. It is safe and convenient to use compared to the conventional clinical way of brain activity measurement which involves the invasive surgical implantation of electrodes in the human brain.

EEG measures voltage fluctuations resulting from the ionic current flows within neurons in the brain. Normal EEG signals are at low frequency band and the normal EEG magnitude is at tens of micro voltages.

2.1.2 Local field potential method

In hospital, the gold standard way to record neural activity is by means of surgical implantation of the electrode in the brain. In the process, the electrode is inserted at the region of interest in the brain to record the so-called local field potential (LFP) which is the low frequency part (below ~ 500 Hz) of the recorded potentials. This technique was used as early as 1875 (Caton, 1875), 50 years before the advent of EEG technique. Although LFP measurement is a promising way to easily reach subcortical brain regions and to record subcortical brain activity, realization of the technique is unsafe. Prior to the insertion of the electrode, the process requires a burr hole drilled in the human skull. The skull tissue being removed is irrecoverable. Furthermore, the insertion of electrode may lead to brain tissue damage to the area around the electrode. As a result, the potential signal picked up by the electrode is highly likely distorted.

During the past decades, EEG has become more and more popular in the field of monitoring brain disorder related diseases. EEG was used to monitor epileptic seizures, to characterize seizures for the purpose of treatment, and to localize the region of the brain where a seizure originates in order to perform possible seizure surgery (Valls-Solé & valldeoriola, 2002; Hallett, 1990; Thomas, et al., 1997). EEG was also used to investigate Parkinson's disease in the early stage (Han, et al., 2013) and hence to provide early treatment to Parkinson patients, which could help delay the progressive neuronal degeneration. However, EEG technique has yet been standardized sufficiently for clinical use and it is most often used for research purposes.

The EEG source localization technique allows a convenient pre-surgical planning based on a non-invasive procedure to provide important information of the localization of epileptic foci for guiding surgical decisions. The technique has been validated and extensively used for the pre-surgical evaluation of patients suffering from refractory epilepsy (Boon, et al., 1997; Krings , et al. , 1999; Merlet, 2001). However, the spatial resolution on the scalp is low thus the neural activity that occurs deep in the brain is poorly determined by EEG. Moreover, data analysis is challenging due to its poor signal-to-noise ratio.

Thanks to the researchers who are dedicating in the algorithm design for effective signal processing, EEG technique is highly possible to become the standard way to monitor and diagnose brain disorder related disease in the deep brain region, and to localize the region of such brain disease.

To achieve this goal, it is of paramount importance to investigate whether EEG could pick up the electrical activity in the subcortical region.

2.2 Brain Source Localization

Brain source localization is to estimate the underlying neuronal sources in the brain through analyzing the potential recordings on the scalp. The process to determine the neuronal sources is to solve the EEG inverse problem.

Throughout the years, many techniques have been developed to solve the EEG inverse problem. Among all the techniques, low resolution brain electromagnetic tomography (LORETA) was found to be the best to utilize.

LORETA technique was originally developed and described by Pascual-Marqui, Michel and Lehman in 1994 (Pascual-Marqui, et al., 1994). This method was developed to localize the electrical activity in the brain based on scalp potentials from EEG recordings. In order to solve the inverse problem accurately, there were some basic assumptions. Firstly, mathematical algorithm of this method was based on a three-sphere head model which consists of a homogeneous medium within each sphere. Secondly, the method assumed neurons that were side by side were synchronously and simultaneously activated. Finally, the inverse solution was based on maximal smoothness and thus the spatial resolution was low.

Nonetheless, LORETA technique gave zero localization error for noiseless, single source simulation (Pascual-Marqui, 2002). Besides that, LORETA was found to give minimum localization errors for noisy data simulation (Pascual-Marqui, 1999). Owing to its excellent capability of brain source localization, LORETA technique was validated through experiment and extensively applied to find activation of visual, auditory and motor cortices (Khateb, et al., 2002; Hirota, et al., 2001; Van, et al., 1998; Mulert, et al., 2001; Anderer, et al., 1998a; Anderer, et al., 1998b). Furthermore, LORETA has also been applied

to find activation of epilepsy (Worrell, et al., 2000; Seeck, et al., 1998; Lantz, et al., 1997).

Although LORETA has been extensively applied for EEG source localization problems, to our knowledge its capability of deep source localization is not well understood. While deep brain source located at subcortical structures such as basal ganglia, hippocampus and thalamus were found important for clinical neurophysiological studies.

In order to expand the use of non-invasive EEG brain activity measurement and then inversely localize the corresponding activation of neuronal activity in clinical neurophysiology, it is encouraging to investigate the deep source localization.

2.3 Existing Head Models

Conventionally, in order to obtain accurate and realistic results, the default testing method for EEG studies should use human as the testing subject. Up to date, the most realistic study of EEG to measure brain neuronal activities on the scalp is by conducting experiments on humans who had electrodes implanted in their brain during surgery (Cooper, et al., 1965; Kuss, et al., 2011). Undoubtedly, these experiments do provide the most accurate materials and anatomic geometries of the human head. However, there are a number of challenges involved in the process of the invasive experiment. Firstly, the high difficulties in surgery execution will cost a large amount of operation fee. Secondly, scalp EEG experiments require a large number of sample sizes due to the variability of neural responses from human. Even the variability within an individual subject can range greatly over the course of a day. In other words, many of these intraoperative experiments have to be conducted on different patients in order to obtain a good representation of the population since these experiments are non-reproducible. Thus, this method is not suggested for this research due to high cost and high risk occurs along the invasive electrode implantation process.

In order to design a low cost and reproducible experiment, the use of a phantom model should be considered. By using the phantom model, the neuronal activities become controllable and hence it enables the EEG hardware and algorithms being tested easily.

The reviewed existing head models include digital models, human cadavers and artificial physical phantoms.

Computer simulation such as Finite Element Analysis (FEA) which is often used for the evaluation of the accuracies of EEG localization studies might be considered in this research due to its flexibility in altering the synthetic neuronal activities (Liu, et al., 2002; Collins, et al., 1998; Nunez & Srinivasan, 2005; Attal, et al., 2009; Wolters, et al., 2006). Besides that, computer simulation generated digital model is an effective tool in controlling every single variable during the experiments. However, it does not capture the realistic electromagnetic interference (Collins, et al., 1998; Wolters, et al., 2006). Besides, all the assumed circumstances which have been programmed into the mathematical methodology in simulation may cause the generation of unrealistic experimental results, which may hence cause the results to be incomprehensive compared to the actual scenario.

By using human cadavers, an anatomically accurate model can be obtained (Barth, et al., 1986; Leahy, Mosher, et al., 1998). However, the lifespan for which a cadaver can be used is limited. Besides that, the electrical conductivities of dead tissue are different from that of living tissue (Miklavcic, et al., 2006), which means the transmission of signals from the brain to the scalp will be different from the real scenario. One of the reviewed phantom head models is in the form of a human skull filled with wax or gelatin (Shmueli, et al., 2007; Greenblatt & Robinson, 1994; Lewine, et al., 1995). The phantom has a high accuracy in anatomical geometries. However, it lacks stability due to the use of the human skull which is actually a dead tissue. Nevertheless, a high anatomically accurate phantom head model is still a good choice for testing. It enables many different kinds of EEG studies to be taken in place.

Current artificial head models utilizing conductive gelatin, agar or carbon doped silicone, urethane (Baillet, et al., 1997; Collier, et al., 2012). Both types present realistic anatomic properties. The former type head model made of conductive gelatin and agar is convenient for fabrication and the latter type head model made of conductive silicone rubber has good stability in material and anatomic properties over time.

In order to build a physical head model with stable property yet convenient to update information, the materials were recombined to form a three layer realistic human head model in later chapters. For the individual chapter, the materials used to construct the head model were different. However it would not affect the material electrical conductivity in the low frequency range. In low frequency band, all materials act as a pure conductive medium and as a result only the electrical conductivity varies. As long as the electrical conductivity value remains consistent, the EEG recordings on the scalp should remain the same.

2.4 Electrical Properties of Brain, Skull and Scalp

The brain is the most complex organ in the human body. It contains one hundred billion nerve cells called Neurons as well as connective cells called Glia (Philips, 2006). It consists of three main parts, which are the forebrain, the midbrain and the hindbrain. The forebrain is responsible for receiving and processing sensory information, thinking, perceiving, producing and understanding language, also controlling motor function. The midbrain connects the hindbrain and the forebrain, and is involved in auditory and visual responses as well as motor function. Lastly, the hindbrain extends from the spinal cord and assists in maintaining balance and equilibrium, movement coordination, conduction of sensory information, as well as controlling autonomic functions such as breathing, heart rate, and digestion (Bailey).

The brain is not only composed of grey matter, but also formed up by white matter. The grey matter is the neuronal cell bodies consist of neural cell bodies, dendrites, capillary blood vessels and unmyelinated axons. It is distributed at the surfaces of the brain. Also, it forms the brain stem, thalamus and basal ganglia.

On the other hand, the white matter is like a branching network which is formed by dendrites and axon spreading out from the cell bodies to connect to other neurons. It consists of glial cells and myelinated axons. Also, it forms the deep part of the brain.

Research has shown that the grey matter has an average electrical conductivity of 0.35 S/m (Gedders & Baker, 1967) while the white matter has an average conductivity of 0.15 S/m (Burger & Milaan, 1943). Thus, these two values

will be used as a reference to reproduce the grey and white matter functional materials in this research.

The structure and thickness of the human skull are inconsistent and vary from one part to the other part. Similarly, the electrical conductivities of the human skull also vary a lot. The anisotropic property of the skull has been a controversial issue as different results related to the skull were obtained under different experimental setup and environment by different researchers.

As studied, the radial electrical conductivities of the skull were measured as 0.00118 S/m at outer cortical bone, 0.00773 S/m at cancellous bone and 0.00332 S/m at inner cortical bone by Akhtari and his team (Akhtari, et al., 2002). For live tissues, the conductivities were a factor of 1.5 to 5.2 times larger, about 0.00487 S/m at outer cortical bone, 0.0214 S/m at cancellous bone and 0.00617 S/m at inner cortical bone.

For the following studies, the lowest conductivity of live tissue from human skull, 0.00487S/m will be used as the minimum acceptable electrical conductivity to build the skull layer.

On the other hand, research has also shown that the skull has a radial electrical conductivity of 0.01 S/m (Oosten, et al., 2000). This value again will serve as the reference for the making the skull layer.

The scalp is a specialized area of skin on top of the head. It consists of five layers namely the Skin, Connective tissues, epicranial Aponeurosis, Loose areolar tissue and the Pericranium (Harris, 2013). The aforementioned first three layers are bound together and can move along the loose areolar tissue over the pericranium, which is adherent to the calvaria. The scalp covers most of the head, starting at the top of the forehead, and contains as many as 150,000 hair follicles. Research has shown that the scalp exhibits an averaged conductivity of 0.43 S/m (Burger & Milaan, 1943).

2.5 Concluding Remarks

Much different from the literature surveyed physical head models which have been utilized for cortical neuronal activity studies, the subcortical emphasized physical human head model developed in this research aims for evaluation of the subcortical and deep brain source contribution to scalp EEG recordings. To our knowledge, this model is the world's first physical head model designed for subcortical and deep brain source localization studies. The novelty of this head model is attributed to the location design of its artificial neuronal sources. The artificial neuronal sources were distributed not only in the brain cortex, but also in the subcortical region and deep brain. Specifically speaking, three artificial neuronal sources were respectively distributed in corpus callosum, thalamus and hypothalamus in the subcortical region. Besides, two more artificial neuronal sources were designed to distribute in the brain stem including the midbrain and pons.

CHAPTER 3

General Experiment Methods

In this chapter, the materials and methods of making the respective layers of the physical head model is introduced. The methods introduced in the early part describe how to make the testing sample for the subsequent electrical property measurement. The methods introduced in the latter part describe how to construct the final physical human head model with realistic anatomic geometries.

3.1 Materials of the Physical Head Model

3.1.1 Sample preparation of the artificial brain

The artificial brain was made of gelatin doped with sodium chloride (NaCl) to achieve the desired electrical conductivity value. The preparation of the brain material was depicted in Figure 1. The sample gelatin solution prepared by distilled water and gelatin powder was firstly transferred to a beaker and the beaker was placed on a water bath of temperature maintained at $50\text{ }^{\circ}\text{C} \pm 5\text{ }^{\circ}\text{C}$. This temperature level was recommended as a good casting temperature by Kozlov and Burdygina (Kozlov & Burdygina, 1983). There was a thermometer placed inside the sample gelatin solution in order to control its temperature. The water bath was placed on a magnetic stirrer in order to mix the gelatin solution thoroughly with additional chemicals. The magnetic stirring process was maintained for 30 minutes. The fully dissolved solution was transferred to a petri dish and the solution was allowed to gradually cool down to room temperature of $24\text{ }^{\circ}\text{C}$ before stored in the refrigerator overnight.

The next day, the sample was taken out from the refrigerator and placed in the experiment room for gradually warming up to room temperature for the subsequent electrical conductivity measurement.

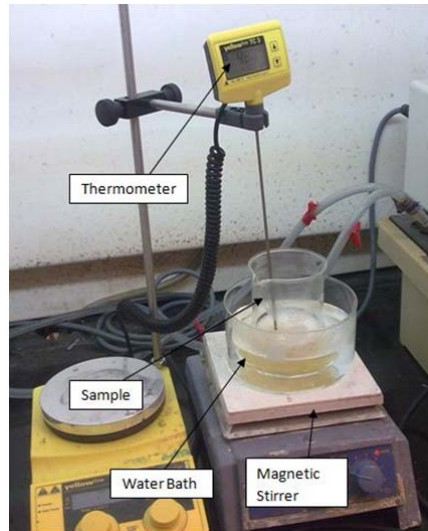


Figure 1: Experimental setup for preparation of gelatin material.

3.1.2 Sample preparation of the artificial skull

The sample skull layer was made of electrically conductive silicone rubber purchased from Square Silicone Co., Ltd. (Shenzhen, China). The desired electrical conductivity was customized. The preparation of the skull material was depicted in Figure 2. The two-part silicone material was mixed at the ratio of 1: 2. Due to its high viscosity, the pre-mixed material was mechanically stirred to achieve a thorough mixture. Next, the well mixed material was placed in the vacuum chamber to allow air bubbles released from the viscous material. After air bubble release, the material was injected into an aluminum mold which was designed to produce a sample piece with thickness of 7 mm. The mold was subsequently placed in the oven (temperature maintained at

100 °C) to facilitate cure. The sample was then placed in the experiment room to gradually cool down to room temperature for the subsequent electrical conductivity measurement.

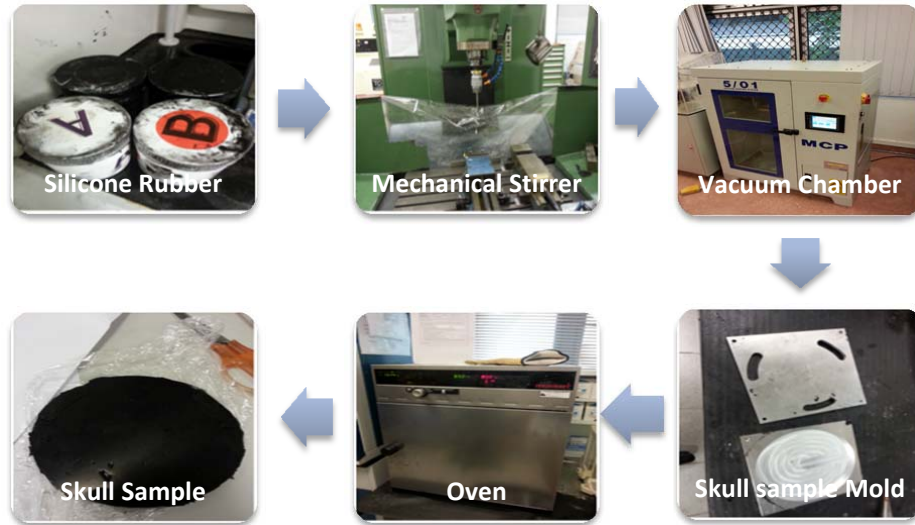


Figure 2: Flowchart of how to make the skull sample.

3.1.3 Sample preparation of the artificial scalp

According to Leahy and et al. (Leahy , et al., 1998), the scalp layer could be prepared by coating 40 layers of the liquid latex rubber on the skull layer to achieve an approximate thickness of 5 mm. The same coating method was adopted in this research study to make the artificial scalp layer. The pure liquid latex rubber was purchased from Castin's Craft brand (Mold Builder, California, USA). In order to achieve the desired electrical conductivity, the liquid latex rubber was doped with NaCl prior to coating layer by layer. The preparation of the scalp material was depicted in Figure 3. Firstly, NaCl (12.5 g) was pre-dissolved in the distilled water (60 ml) and then doped into the

liquid latex rubber material (300 ml). Owing to its viscous property, the sample liquid was then mechanically stirred for 5 min to ensure NaCl solution thoroughly mixed with liquid latex rubber. Third, the artificial scalp was formed by coating the fully prepared sample liquid layer by layer on a petri dish. In the coating process, each coat was allowed oven dry (temperature maintained at 100 °C) and cured before the next coat. In total, 40 layers were coated to achieve an approximate thickness of 5 mm. After the last layer was coated and cured, the sample was allowed to gradually cool down to room temperature. Finally, the sample was wrapped with the cling film (Phoon Huat & Co Pte. Ltd., Singapore) and stored in the refrigerator. The final step was to prevent the sample not only from drying, but also from airborne contamination. Thus, the electrical conductivity of the sample was maintained for a certain period and the usage life of the sample was prolonged. The sample was taken out from the refrigerator and placed in the experiment room for gradually warming up to room temperature for the subsequent electrical conductivity measurement.

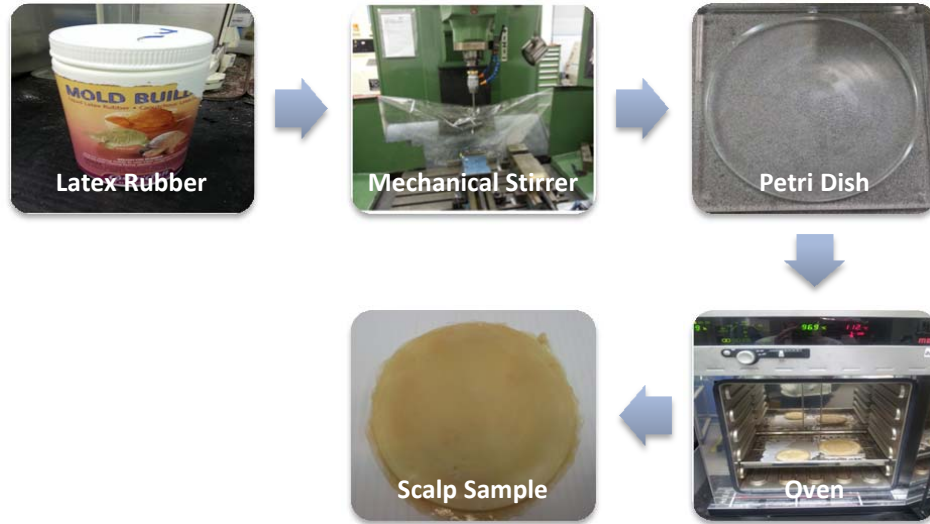


Figure 3: Flowchart of how to make the scalp sample.

3.2 Electrical Property Measurement

The general electrical property measurement aims to measure the electrical conductivity of the testing samples. The testing samples refer to the artificial brain, skull and scalp. As shown in Figure 4 (a), the testing sample was placed in between two copper electrodes which were affixed on the testing fixture. Dimension of the electrode was 10 mm in diameter (\varnothing). The four corner screws were used to make sure the two electrodes were directly facing each other. Therefore, the electrode center-to-center distance (d) was taken to calculate the electrical conductivity of the testing sample. The two electrodes were then connected to the LCR meter (3522-50 LCR HiTESTER, HIOKI, Japan) for impedance measurement (Figure 4 (b)). An LCR meter is an electronic test equipment used to measure the inductance (L), capacitance (C) and resistance (R) of a testing sample. In this research, the input voltage and frequency were set at 3 V and 10 Hz respectively. The voltage level was

chosen arbitrarily, however the frequency level was chosen according to that was given to the dipole source embedded in the physical head model. This LCR instrument read impedance reading (Z) instantly. Given the impedance reading, electrical conductivity (σ) of the sample was calculated by equations (3.1) and (3.2).

$$\sigma = \frac{d}{Z \times A_{surface}} \quad (3.1)$$

$$A_{surface} = \frac{\pi \phi^2}{4} \quad (3.2)$$

where $A_{surface}$ is the contact area between the electrode and testing sample.

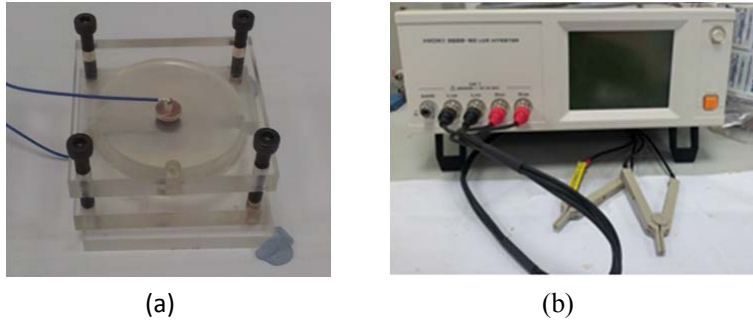


Figure 4: (a) Sample impedance testing fixture and (b) LCR meter for impedance measurement.

3.3 The Physical Head Model

The physical head model was a three-layer model which was composed of the artificial brain, skull and scalp. Inside the brain layer, a current dipole source was pre-embedded to simulate the underlying neuronal source activity.

Construction of the physical head model was realized with four procedures namely computer-aided design, rapid prototyping, casting and injection

molding. The three-dimensional (3D) brain and skull models were originally purchased from AnatomiumTM (21st Century Solutions Ltd). The original models were modified in this research. The initial surface models of the 3D brain and skull were converted to solid models using SolidWorks software (SolidWorks Corporation, Waltham, MA) in order to send for rapid prototyping. The complicated brain surface geometries of sulcus and gyrus were preserved. Furthermore, the 3D brain and skull models were trimmed and scaled to fit each other properly. There was no 3D computer-aided design model of the scalp since the scalp layer would be fabricated by coating the pure liquid latex on the final skull layer. Due to the complicated geometries of the brain surface, the aforementioned non-conventional rapid prototyping manufacturing method was applied for fast and convenient master pattern production. The master patterns would then be used for mold making. As introduced earlier on, casting method was also applied in this research. In particular, the aluminium mold was casted to eventually form the outer surface geometry pattern of the skull layer, while the inner surface geometry was formed by the brain master pattern (see Figure 5). The cavity formed the shape of the skull layer with injection of the electrically conductive silicone rubber material.

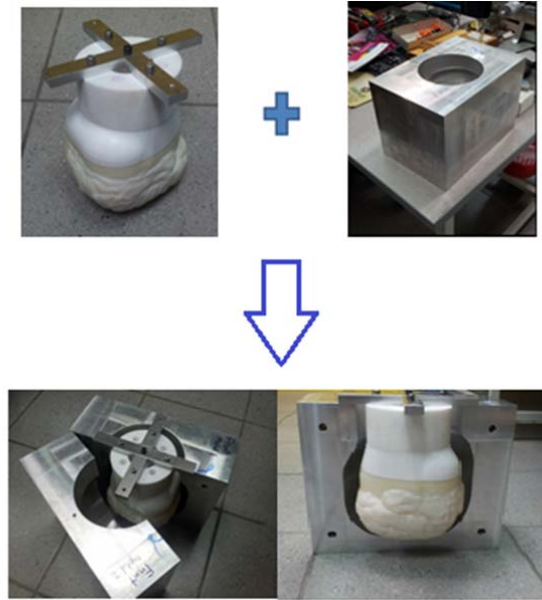


Figure 5: Assembly of the brain master pattern and the aluminium mold.

3.4 Electroencephalography Measurement

EEG signals measured on the scalp was recorded with a WaveGuard 64 EEG cap and using the ANT amplifier system (Advanced Neuro Technology, Enschede, Netherlands). The experiment setup required the injection of EEG electro-gel (Electrogel, Electro-Cap, International, Inc., Eaton, OH) at each electrode cup. The electro-gel ensured good electric conductance between the electrode cup and the underneath scalp. In the experiment, the input impedance values of all channels were checked no larger than 2 k Ω throughout the whole recording session. The sampling rate of data acquisition was 250 Hz. The electrode sites placed on the scalp were in accordance with the extended international 10-20 electrode placement system (Jurcak, et al., 2007). All channels were referenced to the common average. EEG data were recorded and real-time displayed using asalab™ EEG acquisition software.

Collected data were off-line examined and processed using asa™ signal analysis software.

3.5 Low Resolution Brain Electromagnetic Tomography

Low resolution brain electromagnetic tomography (LORETA) method determines the relative activity of regions in the brain based on the EEG recordings captured by surface electrodes along the scalp (Pascual-Marqui, 1999). Unlike EEG is the recording of electrical potential differences on the scalp, LORETA method computes the distribution of the current source density in the brain. A newer version of LORETA is called standardized LORETA. It is capable of localizing test point sources with zero localization error in the absence of noise. In this research, sLORETA analysis was utilized for the study. However, most often the term LORETA was mentioned in the research. It does not make any confusion since sLORETA method belongs to the LORETA family. The analysis is based on a three layer spherical model. Following the steps to select the correct entries, the sLORETA free academic software would compute the dipole source locations in a brain atlas.

CHAPTER 4

Electrical Characteristic Study of the Artificial Brain Material

Brain occupies most of a human head and its underlying neuronal activities are of great interest to neurophysiologists who are studying brain functions such as memory and emotion. Brain is composed primarily of two broad types of cells, neurons and glial cells. Glial cells play a role to provide critical functions including structural support, metabolic support, insulation and guidance of development. Neurons are considered even more important as they make successful signal transmission and signal exchange among neurons to form the complicated neural network. Paying attention to the important role of brain, this chapter gives a comprehensive study on the electrical characteristics of the artificial brain material.

4.1 Introduction

Recently, functional neuroimaging methods such as the functional magnetic resonance imaging (fMRI) and multichannel electroencephalography (EEG) are widely used for the localization of neural sources (Li & Duc, 2012; Indiradevi, et al., 2008). The recording speed of fMRI is slow. Thus, for real time recordings, EEG method is more appropriate to apply owing to its excellent temporal resolution. The method to solve the EEG inverse problem is to use the equivalent current dipole and clusters of such dipoles as the source model, and estimate the locations and amplitudes of the equivalent current dipoles. The EEG inverse problem is also well known as the source localization problem. The objective to solve the source localization problem is

to assess the accuracy of the estimated source location with known true location and temporal activity of the dipoles. Solving the source localization problem includes challenging design of algorithms. If the algorithms are proved to correctly give the source location, then it would have wide applications in neurophysiological studies.

The first step to tackle the source localization problem is to establish a forward model. This step involves recording of the scalp potentials from electrodes placed on a head model for a given predefined dipole source. Considering the head model in neurophysiological studies, the human head is modeled as a three layer volume conductor (Rush & Driscoll, 1968). This volume conductor is composed of brain, skull and scalp. Each layer plays a unique role when considering the electrical field spreading across each layer and EEG signals received on the scalp. Brain functions as a weak conductor, as well as the location where neuronal activities originated. Skull is taken as a low-pass filter owing to its poorer electrical conductivity compared to brain and scalp. Furthermore, the poor electrical conductivity of the skull leads to significant attenuation of the electrical field passing through the human head. While talking about scalp, it is in direct contact with the measuring electrodes and significant experimental noise is incurred on scalp. With the unique role of each layer of the human head in mind, before going to develop the physical head model, first priority was given to the electrical characteristic study of the artificial brain material.

According to the existing research, in neurophysiological studies gelatin is popularly used to mimic the brain tissue because of its physical characteristic that resembles the structure of human connective tissue (Baillet, et al., 2001;

Kuss, et al., 2011; Leahy et al., 1998; Spencer, et al., 1996). To our knowledge, previous electrical characteristic study on gelatin based conductive electrolyte was examined in the low frequency range by Zhou (Zhou, et al., 2007). However, the behavior in high frequency range remains unknown. In 1990, electrical characteristic study of the pure gelatin was carried out and used for simulation of biological tissues (Nadi, et al., 1990). However, the pure gelatin contains no freely moving electrical ions as those found in neuronal activities. Thus, introduction of sodium and chloride ions is necessary to better simulate the human brain tissues.

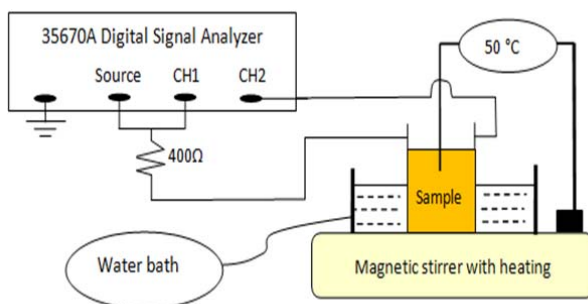
This study aims to investigate the electrical characteristics of the gelatin sodium chloride (gelatin-NaCl) electrolyte corresponding to various frequencies (10 Hz - 50 kHz), sodium chloride (NaCl) concentrations, and temperatures. Different from Zhou's work (Zhou, et al., 2007), the electrical characteristic study was performed both in low and high frequency ranges. Furthermore, an empirical model has been firstly introduced to predict the electrical conductivity of gelatin-NaCl electrolyte with respect to temperature (25 - 50°C) and frequency (10 - 800 Hz).

4.2 Materials and Methods

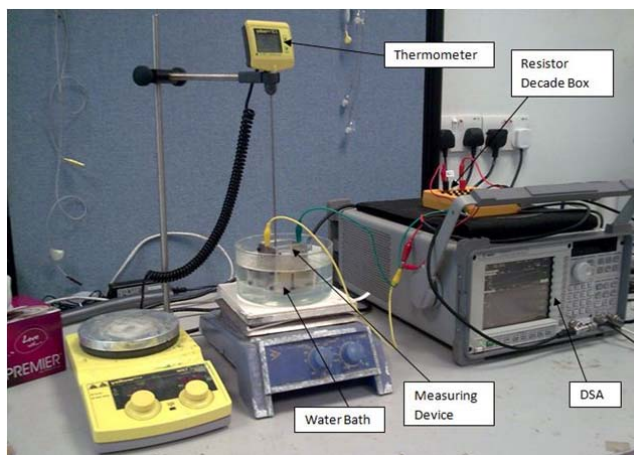
4.2.1 Gelatin-NaCl electrolytes

Different amount of NaCl (0.02 g, 0.09 g, 0.5 g and 0.9 g) was mixed with 20 g of gelatin (200 Bloom) and 0.05 g of preservative sodium benzoate. The mixture was then dispersed into 80 ml of distilled water. In this study, approximate 20% (percentage weight/weight) concentration of gelatin was chosen because it provided greater strength than 10% concentration of gelatin

(Jussila, 2004). As shown in Figure 6, the solution was prepared in a water bath (temperature maintained at $50\text{ }^{\circ}\text{C} \pm 5\text{ }^{\circ}\text{C}$) and was magnetic stirred at low speed for 30 minutes until complete dissolution was achieved. The solution was then gradually cooled down to room temperature and conditioned for 72 hours before use.



(a)



(b)

Figure 6: (a) Schematic drawing of the experimental setup and (b) the real experimental setup for impedance spectroscopy measurement under different temperature levels.

4.2.2 Impedance spectroscopy measurement

Ionic conductivity of the electrolyte and its frequency response behavior were determined by the impedance spectroscopy measurement. A rectangular chamber made of acrylic was used to measure the electrolyte with two aluminium plates acting as electrodes. The circuit diagram was depicted in Figure 7. The two electrodes were connected in series to Agilent 35670A Digital Signal Analyzer (DSA) with an applied sinusoidal voltage source of 5 V peak-to-peak in the frequency range of 10 Hz to 50 kHz. A resistance of 400 Ω was connected in series to the DSA. The electrolytes were first heated up to 60 °C in a water bath to a liquid state and cooled down subsequently. The electrolytes were measured at 50 °C, 45 °C, 37 °C, 30 °C, and 25 °C. Voltage ratio and phase angle were obtained from the DSA and converted to ionic conductivity. Since conductivity is the reciprocal of resistivity, therefore by using this relation, conductivity can be determined through the derivation

$$\sigma = \frac{L}{Z \times A_{surface}} \quad (4.1)$$

where L (50.7 mm) is the distance between the two electrodes, Z is the impedance of the electrolyte and $A_{surface}$ (608 mm²) is the surface area of the electrodes that is in direct contact with the electrolytes. Each measurement was repeated for three times strictly under the same condition and procedures so as to verify repeatability of the measurement. Averaged values were presented in the following sessions.

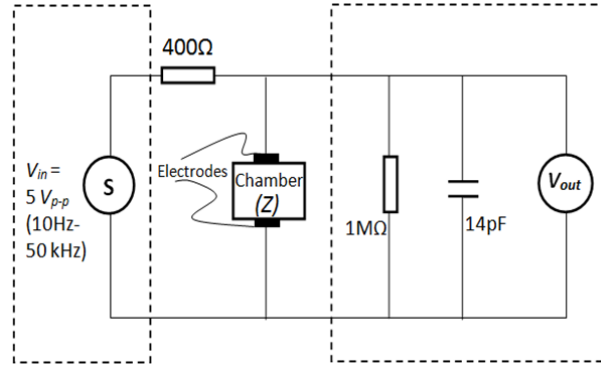


Figure 7: Circuit diagram for impedance spectroscopy measurement of the gelatin-NaCl electrolyte using digital signal analyzer (dotted box indicates the internal circuitry of the analyzer).

4.3 Results and Discussion

4.3.1 Impedance spectroscopy measurement

Impedance spectroscopy has been used to characterize the ionic conductivity of the gelatin-NaCl in response to the frequency range from 10 Hz to 50 kHz. Figures 9 - 12 display frequency (logarithmic scale) and temperature dependence of the ionic conductivity with the four various concentrations of NaCl respectively.

The results could be summarized as follows: for each figure with a particular temperature, ionic conductivity increases sharply in the low frequency region, from 10 Hz up to 500 Hz, while it starts to saturate from 500 Hz to 50 kHz. Across the four figures, it is observed that ionic conductivity increases as the concentration of NaCl increases. It is clear that the magnitude of ionic

conductivity is found to be 0.42 S/m with NaCl concentration of 0.02g/80ml compared to 1.07 S/m with that of 0.9g/80ml measured at 37°C, 800 Hz.

4.3.2 Temperature dependence of ionic conductivity

Figure 8 shows the temperature dependent ionic conductivity at four frequencies (100, 250, 500 and 800 Hz) in the temperature range of 25 - 50 °C. At each frequency, ionic conductivity of the electrolyte is linearly proportional to temperature. This linear relationship was validated by the linear curve fitting results R^2 values. The minimum R^2 value was found to be 0.9976.

Two reasons can be used to describe the results mentioned before. First reason, as frequency increases, with temperature kept constant, more energy are transmitted to the sodium ions and chloride ions, causing the ions to be more active, which implies lower resistance faced by the ions as they are actively mobile. Since conductivity is reciprocal of resistivity, this implies the lower the resistance, the higher the conductivity is, thus causing the overall conductivity of the gelatin-NaCl electrolyte to rise. This conclusion can be seen in Figure 9; as frequency increases, the conductivity of the electrolyte at a constant temperature increases, where the highest ionic conductivity for 50°C reaches 0.62 S/m as compared to the lowest of 0.07 S/m. However, saturation level is reached when the ions mobility is at its limit whereby higher frequency or more energy has no effect on it. These cause the ionic conductivity of the electrolyte to saturate at around 13 kHz in Figures 9 - 12.

Second reason, as temperature rises, with frequency kept constant, the volume in the gelatin-NaCl electrolyte expands and creates free spaces within the electrolyte. These free spaces results in higher ions mobility, thus increasing

the overall conductivity of the electrolyte as temperature rises (Hatta, 2009; Rajendran & Uma, 2000). This conclusion can be seen in Figure 8, at a fixed frequency, the conductivity of the electrolyte increases linearly as temperature rises.

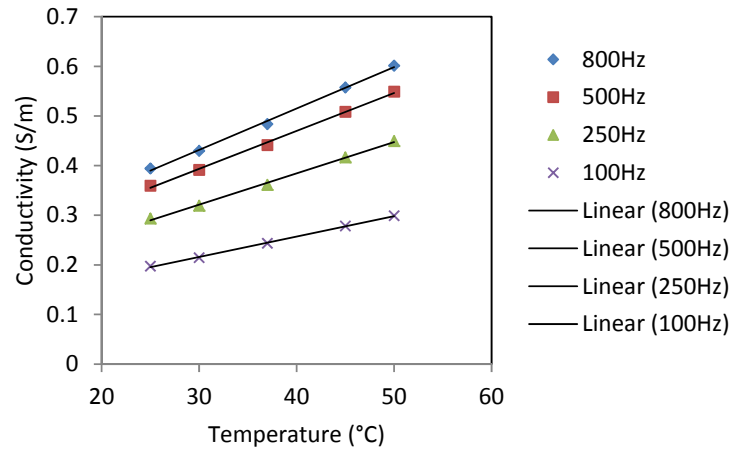


Figure 8: Ionic Conductivity of gelatin-NaCl is linearly proportional to temperature (100 - 800 Hz with 0.09g/80ml NaCl).

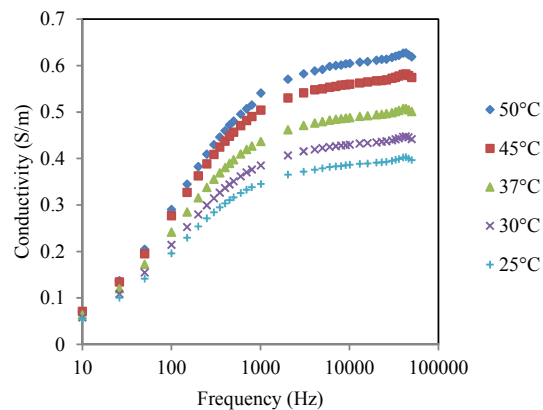


Figure 9: Ionic Conductivity of gelatin-NaCl as a function of frequency (25-50°C with 0.02g/80ml NaCl).

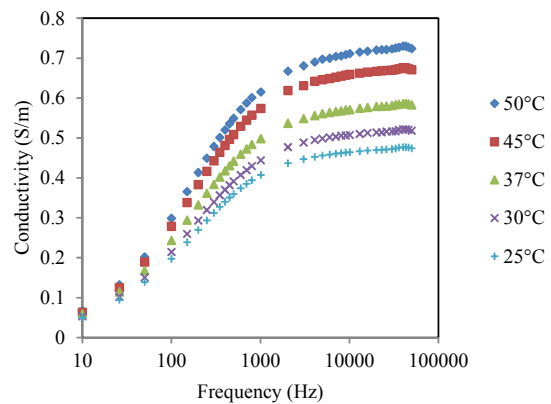


Figure 10: Ionic Conductivity of gelatin-NaCl as a function of frequency (25-50°C with 0.09g/80ml NaCl).

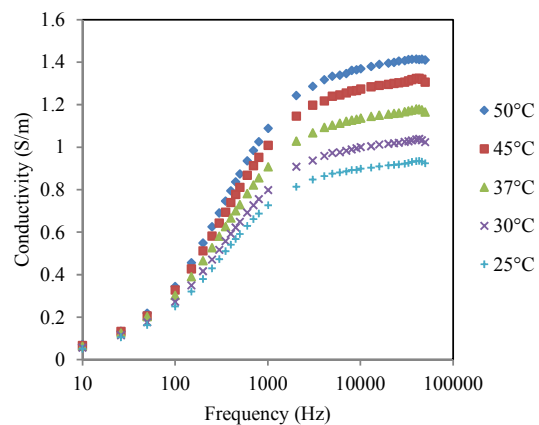


Figure 11: Ionic Conductivity of gelatin-NaCl as a function of frequency (25-50°C with 0.5g/80ml NaCl).

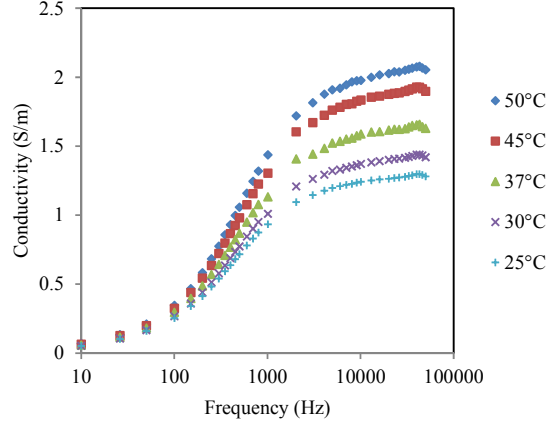


Figure 12: Ionic Conductivity of gelatin-NaCl as a function of frequency (25-50°C with 0.9g/80ml NaCl).

4.4 Empirical Model

Mathematical analysis is proposed to predict the ionic conductivity of gelatin-NaCl electrolyte with respect to temperature (25 - 50 °C) and frequency (10 - 800 Hz). The analysis is first conducted for the electrolyte with specific NaCl concentration of 0.09g/80ml and in the low frequency range of 10 - 800 Hz where a sharp ionic conductivity change is observed. Supported by the observation of Figure 8, the ionic conductivity is a linear function of temperature represented by

$$\sigma = A \times T + B \quad (4.2)$$

where σ is the ionic conductivity (S/m) with NaCl concentration of 0.09g/80ml, T is the temperature (°C), A is a frequency dependent parameter (S/m-°C), and B is another frequency dependent parameter (S/m).

Curve fitting has been done in MATLAB (2010b, The MathWorks Inc., Natick, Massachusetts) using simple linear regression method (Draper & Smith, 1998). The most suitable expressions obtained for parameters A and B are

$$A = af^b + c \quad (4.3)$$

$$B = \gamma - \alpha e^{-\beta f} \quad (4.4).$$

Where f is the frequency. These two expressions are subsequently applied for the electrolytes with NaCl concentrations of 0.02g/80ml, 0.5g/80ml, and 0.9g/80ml. For each concentration, results of the coefficients a , b , c , γ , α , and β are summarized in Table 1 and Table 2. The worst goodness of fit value is larger than 98% among the eight curve fittings, four fittings for parameter A and another four fittings for parameter B . Figure 13 displays the experimental data compared to the fitted lines, which indicates good curve fitting results for ionic conductivity as a function of temperature and frequency.

Table 1 Curve fitting results of a , b , and c .

Concentration of NaCl (g/80ml)	a (S/m-°C-Hz)	b	c (S/m-°C)
0.02	0.03579	0.03794	-0.03865
0.09	0.01317	0.09417	-0.01605
0.5	0.00094	0.42730	-0.00239
0.9	0.00025	0.65310	-0.00086

Table 2 Curve fitting results of γ , α , and β .

Concentration of NaCl (g/80ml)	γ (S/m)	α (S/m)	β (1/Hz)
0.02	0.15530	0.11600	0.00649
0.09	0.18140	0.14350	0.00436
0.5	0.35930	0.31650	0.00398
0.9	0.43520	0.40430	0.00368

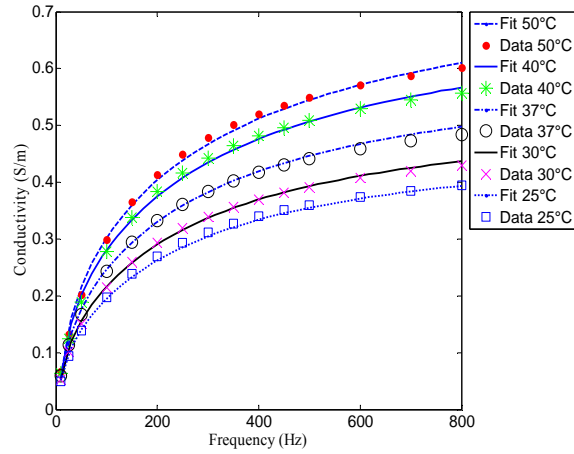


Figure 13: Curve fitting lines (dotted lines) versus experimental data (25-50 °C, 10-800Hz with 0.09g/80ml NaCl).

4.5 Concluding Remarks

Electrically conductive electrolytes based on gelatin and NaCl were prepared and their electrical characteristics were examined. The results indicated that ionic conductivity of this electrolyte is influenced by frequency, the amount of NaCl and temperature. The result of ionic conductivity as a function of temperature exhibited a linear relation. Different from Zhou's work (Zhou, et al., 2007), electrical characteristic study has been performed both in low and high frequency ranges in this research. In addition, an empirical model that predicts ionic conductivity of gelatin-NaCl electrolyte with respect to temperature (from 25 to 50°C) and frequency (from 10 to 800 Hz) has been established for the first time. The results suggest that the low cost gelatin-NaCl is a good tissue replica that mimics brain tissue with a specific ionic conductivity.

CHAPTER 5

Evaluation of the Performance of A Head Phantom System for Event-Related Potential Studies

In this chapter, the reliability to use the physical head phantom was evaluated prior to the brain activity measurement and brain source localization studies which would be introduced in chapter 6 and chapter 7.

5.1 Introduction

There are continuing needs to develop a human head phantom system in the field of electroencephalography (EEG) studies. This phantom system could be used to evaluate EEG recordings and to determine the inverse algorithm of the EEG source localization studies. Researchers have proposed the use of a phantom to replace human test subjects. The main advantage of using the phantom is that the neural source signal as well as the responsive scalp potential recordings becomes controllable. Evaluation of EEG forward and inverse algorithms as a result becomes promising using the phantom.

Existing phantom approaches include digital models, testing conducted on patients during epilepsy surgery, human cadaver based models and artificial head models (Liu, et al., 2002; Cuffin, et al., 1991; Spencer, et al., 1996; Collier, et al., 2012; Okano, et al., 2000; Cao, 2006; Lazebnik, et al., 2005). Each of these phantom systems shows its advantages and disadvantages. Using digital models is the most effective way to study source localization problems. However, it does not capture any environmental noise (Cao, 2006). Testing conducted on patients during surgery though has the most accurate

material and anatomic properties, and encounters many challenges (Cuffin, et al., 1991; Cooper, et al., 1965). The invasive experiments are not reproducible, and require a large sample size to ensure accurate results. Thus the invasive way is costly. The human cadaver based models provide anatomic property accuracy, yet the dead tissue impedance varies a lot from that of the live tissue (Spencer, et al., 1996; Leahy, et al., 1998; Barth, et al., 1986). Current artificial head models utilize conductive gelatin, agar or carbon doped silicone, urethane (Collier, et al., 2012; Marchal et al., 1989). Both types present realistic anatomic properties. The former type is convenient for fabrication and the latter has good stability in material and anatomic properties over time. The existing artificial head model generally provides the underlying dipole sources with arbitrary waveforms (Collier, et al., 2012; Marchal, et al., 1989) to generate so called realistic EEG signals on the scalp. Nevertheless, none of them show the reliability of the generated scalp EEG signals.

This research study aims to evaluate the human head phantom system created for event-related potential (ERP) studies. ERP is a derivative of EEG. Our approach is to compare the correlation between the experimental ERP results and the pre-defined sample ERP data. The pre-defined sample ERP data are taken from one of the case studies in the standardized low resolution brain electromagnetic tomography (sLORETA) software library (Pascual-Marqui, 2002; Fuchs, et al., 2002).

5.2 Materials and Methods

The human head phantom system was composed of the realistic human head phantom, the dipolar sources and the scalp EEG recording equipment (Figure 14). Signal of the dipolar sources was either the pre-defined pulse waveform or an arbitrary sinusoidal waveform. The former pre-defined source waveform was generated by LabVIEW 8.0 software (National Instruments Corporation, Austin, Texas) connected to the dipole signal output driver, while the latter arbitrary sinusoidal waveform was generated by the sinusoidal signal generator (Agilent 33220A Function Waveform Generator, Agilent Technologies, Inc., Santa Clara, CA).

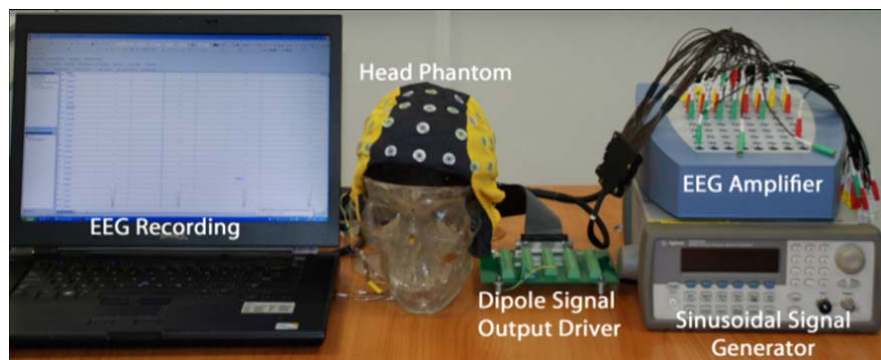


Figure 14: The human head phantom system.

5.2.1 Realistic human head phantom

The head phantom developed in this research study was composed of three layers, namely the artificial brain, skull and scalp. Development of the head phantom was described as follows. The first step involved three-dimensional (3D) design of the head model. Both the brain and skull computer-aided design (CAD) models originally purchased from AnatomiumTM (21st Century Solutions Ltd) were trimmed. The brain model was trimmed and scaled to fit the skull CAD model cavity using SolidWorks software (SolidWorks Corporation, Waltham, MA). We preserved the unique brain surface features of sulcus and gyrus, and filled up its hollow cavities. In this particular study, the skull CAD model was also trimmed to preserve skull cap and the rest was cut. The scalp model was created by scaling up the skull cap. The three 3D CAD models were created for mold making. In order to position dipolar sources in the brain, an antenna support structure was created using SolidWorks software. Figure 15 depicted the assembly of the head phantom including the scalp, the skull, the brain, the antenna support structure and their alignments. The aforementioned CAD models were sent to rapid prototyping process. It was noted that the real scalp 3D CAD model was only the upper half of the head. The full head shape shown in Figure 15 was for convenient visualization to the readers.



Figure 15: Assembly of the three-dimensional design of the head model.

The second step was to prepare materials for the artificial brain, skull and scalp. For convenient head model fabrication and cost saving, in this particular study, gelatin, genipin, sodium chloride (NaCl), deionized water and preservative sodium benzoate were the ingredients for making the artificial brain. NaCl was utilized to adjust the material electrical conductivity to the expected value. The cross-linking agent genipin was utilized to improve the material's stability in terms of electrical and geometric properties. Agar powder and deionized water were the ingredients for making the artificial skull. The scalp layer utilized almost the same ingredients as brain did except genipin. The compositions of the artificial brain, skull and scalp were listed in Table 3.

Table 3 Compositions of the artificial brain, skull and scalp (all units are grams).

	Gelatin	Genipin	Agar	Deionized Water	NaCl	Sodium Benzoate
Brain	175	4.375	-	700	17.6	0.4375
Skull	-	-	18	600	-	-
Scalp	125	-	-	500	12.57	0.3125

Electrical conductivities of the artificial brain, skull and scalp layer were measured before evaluation of the phantom system. The testing method was described in Chapter 3 section 3.2 in detail. Each layer was prepared with three samples on different dates. The results shown in Figure 16 were averaged results and the red error bars indicated the standard deviations showing how widely values were dispersed from the average values. The electrical conductivities of the artificial brain, skull and scalp prepared in this particular research study were 0.302 ± 0.021 , 0.006 ± 0.0004 and 0.160 ± 0.023 S/m respectively.

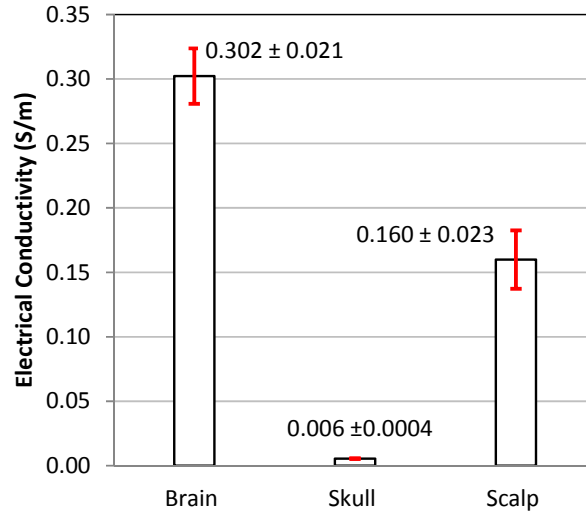


Figure 16: Averaged electrical conductivities of the artificial brain, skull and scalp materials. Red error bars indicated the standard deviations.

In the fabrication process, rapid tooling and casting methods were applied to create the brain, skull, and scalp layer. The brain was the first component to be made. The brain rapid prototype was utilized as the master pattern to make the brain silicone mold. The brain material was then injected into the silicone mold cavity and the brain layer was formed with complicated geometries of sulci and gyri as shown in Figure 17. The artificial brain was stored in the refrigerator overnight to ensure the material was thoroughly solidified. Next we carefully positioned the skull rapid prototype to cover the artificial brain. Markers were created to ensure the head midlines were coincided. The skull material was injected into the cavity between the artificial brain and skull prototype. The agar material of artificial skull solidified fast as the material cooled down to room temperature. The last step was to repeat the previous step to fabricate the scalp layer.



Figure 17: The final brain prototype.

5.2.2 Dipolar sources and ERP recordings

As mentioned earlier, signal of the dipolar sources was either the pre-defined pulse waveform or an arbitrary sinusoidal waveform. In the former case, the pre-defined pulse waveform was the dipolar source waveform taken from sLORETA case studies. The software package of sLORETA provided visual ERP data of seventeen subjects. Due to the inter-subject variability, visual ERP data of one subject were randomly chosen for this research study.

The location of the pre-defined dipole was at Talairach space (+5 mm, -70 mm, -5 mm), occipital lobe, lingual gyrus. Talairach coordinates, also known as Talairach space, was a three-dimensional coordinate system of the human brain, which was used to map the location of brain structures independent from individual differences in the size and overall shape of the brain. The dipolar source was created using a coax cable. Its central wire was exposed 1 mm long and the outer wire was exposed 2 mm long. These exposed tips, were separated by 4 mm distance. The dipolar source was guided by an antenna support structure and the dipole tip was normal to the occipital cortex. To generate the source signal, the other end of the coax cable was connected to NI CB-68LP connector block. The analog output signal was then generated

using LabVIEW 8.0 software and was driven by NI DAQCard-6036E driver software (National Instruments Corporation, Austin, Texas). The original dipolar source waveform was sampled at 256 data points in a 1 second time window (see Figure 18). In order to increase its resolution, the original source waveform was smoothed using cubic spline data interpolation method in MATLAB (The Mathworks, Inc., Natick, MA) and its sampling rate was raised to 661 samples per second.

The source signal was played for 30 s and the responsive ERP signals were simultaneously recorded using with a WaveGuard 64 EEG cap, and the ANT EEG system (sampling rate: 250 Hz) (ANT Enschede, the Netherlands). The electrode positions, according to the LORETA case study, corresponded to the standard 19 sites of the international 10-20 system plus FC1, FC2, CP1, CP2, PO3 and PO4 (Jurcak, et al., 2007). EEG electro-gel was injected at each electrode cup (ElectroGel, Electro-Cap, International, Inc., Eaton, OH). During recording, all input impedances were checked no larger than 2 k Ω for all experimental sessions. All channels were referenced to the common average reference and grounded with channel AFz (Jurcak, et al., 2007). The acquired EEG raw data were further processed in EEGLAB (Delorme & Makeig, 2004) and MATLAB softwares.

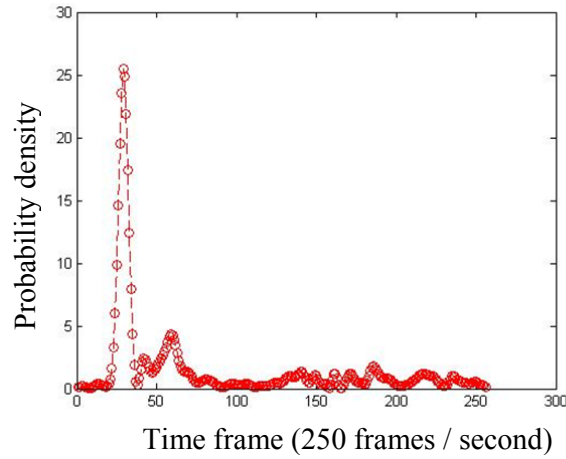


Figure 18: The original dipolar source waveform.

In the latter case where the dipolar waveforms were arbitrary sinusoidal waveforms, the experimental methods were a little bit different. In this case, function generator was used to generate sinusoidal waveforms to the dipolar sources. Each of the 18 dipoles was activated individually with dipolar waveform being an arbitrary sinusoidal waveform (10 Hz, 5 V peak-to-peak). The 18 dipoles were positioned according to the antenna support structure which allowed the 18 dipoles to reach each of the brain functional lobes. Experiments of this case contributed to the forward analysis later.

5.2.3 Forward analysis

The forward model matrix described characterization of the head phantom. To ensure the final prototype was capable of generating expected ERP signals, we evaluated its forward matrix for the three-layer phantom head. The electrode voltages V_{EEG} are the electric potentials recorded by the electrodes on the artificial scalp. The antenna voltages $V_{antenna}$ are the potential difference

between the two poles of each dipolar source. The forward matrix F defined the relationship between the electric potentials recorded by the electrodes on the artificial scalp and potential difference generated by antennas. The forward matrix F was calculated by Equation (5.1) and it was a 25×18 matrix with 25 electrodes and 18 antennas.

$$V_{EEG} = FV_{antenna} \quad (5.1)$$

5.3 Results and Discussion

5.3.1 Forward matrix analysis

The forward model matrix was visualized in Figure 19. Intensity of the electrode response to the antenna source signal was indicated by the color intensity. The dark blue color indicated electrodes with overall low responses to the antenna signals, while the dark red color indicated electrodes with overall strong responses. Antennas named with R were distributed in the right hemisphere. Electrodes on the right half of the scalp were termed by even numbers. On the other hand, antennas named with L were distributed in the left hemisphere. Electrodes on the left half of the scalp were termed by odd numbers. Examining on the forward model matrix, it was found that the electrodes on the right half of the scalp showed strong responses to the underlying antennas in the right hemisphere such as FP2-R1, T8-R6. The electrodes on the left half of the scalp showed strong responses to the underlying antennas in the left hemisphere such as FP1-L1, P7-L8. Besides, the electrode responses were from the frontal lobe, somatosensory cortex,

parietal lobe, temporal lobe and occipital lobe. Therefore, the electrode responses were shown to conform to the pre-defined dipole locations.

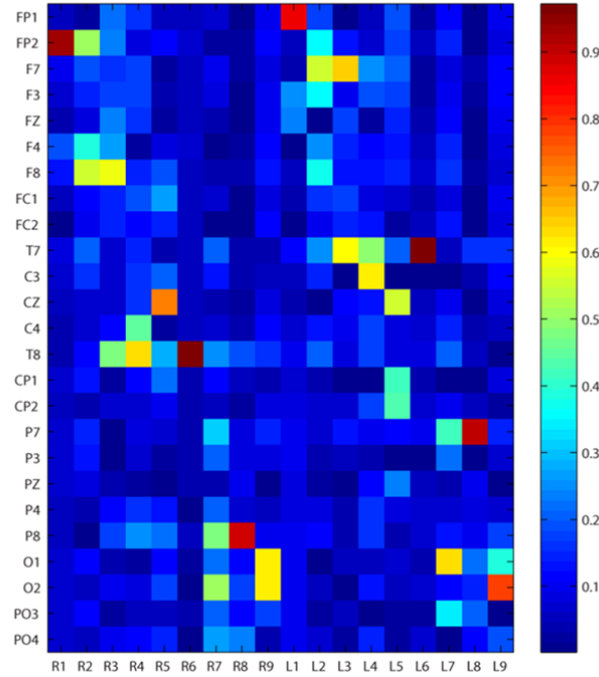


Figure 19: Forward model matrix shows the EEG electrode signal (normalized amplitudes) generated by input sinusoidal waveform (10 Hz, 5 V peak-to-peak) at each of the antenna locations in the head model.

5.3.2 Scalp potential map comparison

The two-dimensional (2D) ERP scalp maps were plotted to visualize 1) the dynamic scalp potential change and 2) the difference between the experimental ERP results and the pre-defined sample ERP data. In Figure 20, two groups of snapshot show respectively the first positive and second positive peak of our experimental results, and the pre-defined ERP data from sLORETA software. The scalp potential maps were drawn by calling EEGLAB function in MATLAB. Experimental results are presented in the upper row, which clearly shows that scalp potential is concentrated at O2

position both for the two peaks. The pre-defined ERP data are presented in the lower row, which shows the scalp potential is roughly symmetric distributed about the brain midline for the first peak while scalp potential is more concentrated at O2 position for the second peak.

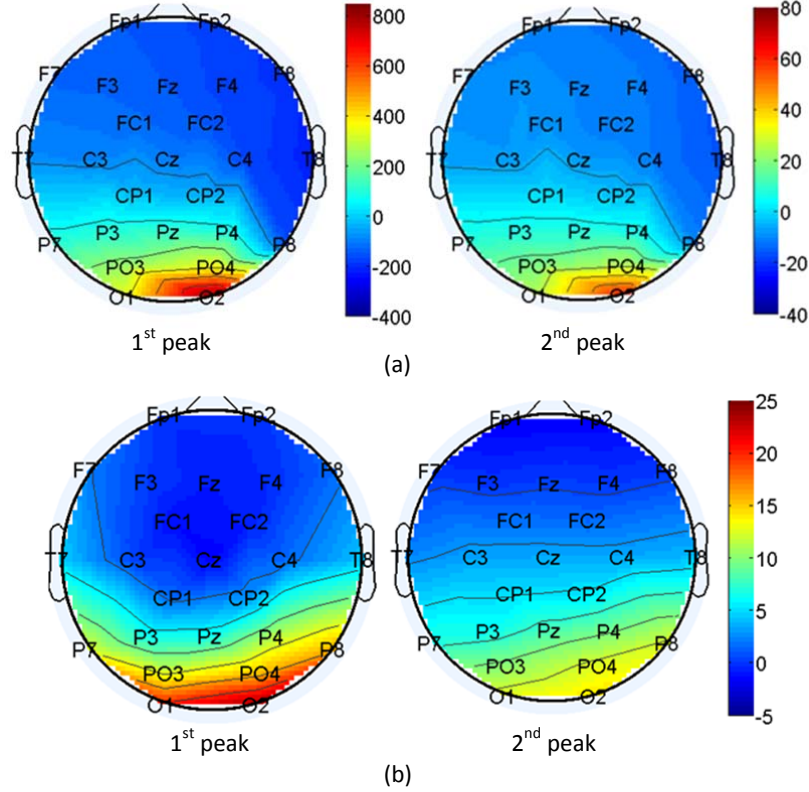


Figure 20: Scalp potential maps (a) experimental results, and (b) LORETA averaged ERP for the 1st peak (left figures) and 2nd peak (right figures). All color bar units: μV .

Besides the brain scalp map comparison, we quantified the relationship between experimental results and the pre-defined data by examining the correlation between them. The Pearson product-moment correlation coefficients are 0.8329 and 0.7906 for the first peak and second peak respectively. The two values show high correlation. Furthermore, P -values are $2.3862e-07$ and $2.5602e-06$ for the two peaks respectively. Both P -values are

much less than 0.05, the 95% confidence level, which indicates significant correlation.

Still, there are differences between the experimental results and the pre-defined data. The differences are explained by the following points. First, in the head phantom there is a deep gap separating the cerebral cortex into the two hemispheres. The design preserves the falx cerebri space and the gap is filled up with the low conductive artificial skull material. In contrast, falx cerebri in a live human head is more conductive compared to the skull. The low conductive artificial skull material obstructs current flow from right to left posterior brain. As a result, we examined the posterior scalp potential was more distributed on the right brain.

Second, we played a single source located roughly below O2 position and that is why the scalp potential is effectively concentrated at O2 position. To improve scalp potential distribution symmetry, one more source is suggested to locate roughly below O1 position and the second source waveform should be carefully designed in future work.

Third, the absolute potential values show large difference. The peak value of the experiment result is 865.2 μV while that of the pre-defined ERP waveform is 24.1 μV . The phenomenon is reasonable because the dipolar source in the experiment was voltage source. In contrast, the pre-defined ERP source signal was probability density. In this research study, the scalp distribution was much more important than the absolute potential value. Therefore, the large absolute value difference is not significant.

Finally, the first and second peaks of the pre-defined results show P100 and P200 respectively. P100 is the first positive component of electrical potential

appearing 100 ms after the stimulus. P200 is the positive going electrical potential that peaks at about 200 ms after the onset of some external stimulus. In other words, the time difference between the first and second peak should be approximate to 100.0 ms. However, the experimental results show the time difference is 460.0 ms, which is not in phase with the pre-defined data. The reason might be due to the increased source waveform sampling rate, 661 Samples/second. The design intended to improve source waveform resolution, yet worsen the result. In future design, we will preserve the source waveform sampling rate as 256 Samples/second.

5.4 Concluding Remarks

This research study has evaluated the human head phantom system created for event-related potential (ERP) studies. Our approach is to compare the correlation between the experimental ERP results and the pre-defined sample ERP data. In the experiment, the dipolar sources were firstly activated with sinusoidal waveforms (10 Hz, 5 V peak-to-peak). The scalp EEG potentials were recorded for the forward matrix analysis. Based on the examination of the forward model matrix, the electrode responses to the underlying dipolar sources were found to conform to the pre-defined dipole locations. Furthermore, the dipolar sources were activated with the pre-defined sample ERP source waveform. Through experiment, the ERP signals were recorded and visualized by the 2D ERP scalp map. Comparing the experimental ERP signals to the pre-defined sample ERP data, significant correlation was observed, i.e. correlation coefficient r : 0.8329 and 0.7906 ; P -value: 2.3862e-

07 and 2.5602×10^{-6} . Therefore, this research study has shown that materials selected and geometric designs of the physical human head phantom were appropriate to use for cortical EEG studies.

CHAPTER 6

Evaluation of Deep Brain Activity Contributing to EEG

6.1 Introduction

Neuronal activity occurring in deep brain structures contains important information of emotions and memories. This deep brain activity is conventionally recorded with surgical implantation of electrodes, during which electrodes are inserted into the brain through the burr hole drilled on the skull. During the neurosurgery process, brain tissue damage and the consequent side effects to patients are inevitably incurred. In order to eliminate undesired risks, we propose that deep brain activity should be measured using the non-invasive scalp electroencephalography (EEG) technique.

EEG is the voltage fluctuation recording of electric activity of neurons along the scalp. In neuroscience studies, electric activity of neurons in a human brain can be considered as electric dipoles, and a human head is considered as a volume conductor. Electric field generated by neuronal activity spreading inside the volume conductor falls off rapidly with distance further away from the dipoles. The deeper the neuronal activity is located, the noisier the corresponding EEG signals are. Activity from deep brain sources becomes more difficult to detect than that from cortical sources. As a result, it is doubted that deep brain activity could be observed from EEG recordings.

Referring to the existing studies, there is statement claiming that the electric field generated by neuronal activity inside the brain is very weak, and the

potential differences caused by dipoles suspended even in mid brain may not be observed on the scalp (Cooper, et al., 1965). On contrary, researchers building inverse models for brain source localization study claim that dipole source activity in the main deep brain structures such as the basal ganglia and the hippocampus may be detected from EEG recordings (Attal , et al., 2009). The existing studies show that the issue pertaining to whether deep brain activity could be observed from EEG recordings has not been confirmed. Therefore, the present study aims to answer this question.

6.2 Materials and Methods

6.2.1 Experiment

In the experiment, a three-layer cylindrical head model was constructed to mimic a human head. The model was 130 mm in diameter and 100 mm in height, comparable to an adult head circumference and height. It was composed of artificial white matter (78 mm thick), grey matter (15 mm thick) and skull compartment (7 mm thick) from bottom to top. The white matter and grey matter were made of sodium chloride mixed gelatin material (Gel strength 300, Type A, Sigma-Aldrich, St. Louis, MO). As for the skull compartment, it was made of liquid latex rubber (Mold Builder, Castin' Craft, California, USA).

The electrical conductivities of the artificial white matter, grey matter and skull were measured using the general testing method described in Chapter 3 section 3.2. The white matter and grey matter were prepared individually for each sample and their electrical conductivities were shown in Figure 21. The

skull compartment was prepared one piece only and was used for all sample tests. Its electrical conductivities tested at three positions were shown in Figure 22. In this research study, the electrical conductivity of each layer was summarized as white matter: 0.16- 0.23 S/m, grey matter: 0.31- 0.39 S/m and skull compartment: 0.002- 0.009 S/m. These values were conforming to the existing research studies (Burger & Milaan, 1943; Gedders & Baker, 1967; Oosten, et al., 2000).

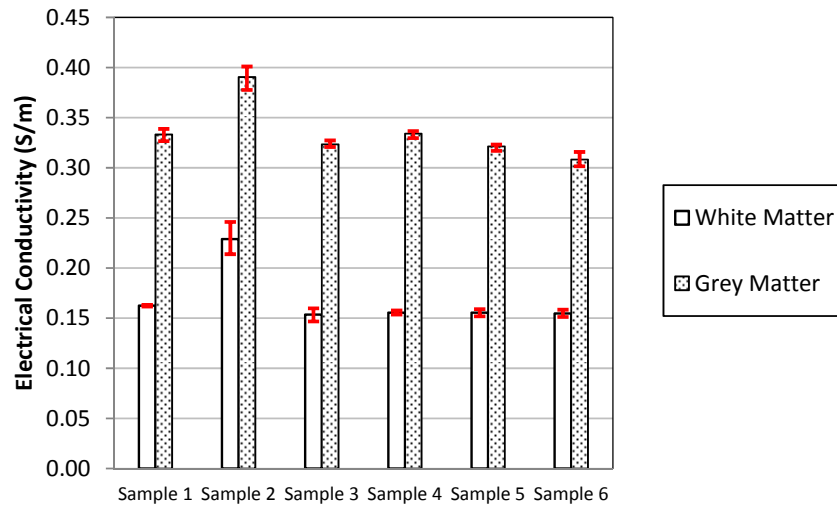


Figure 21: Electrical conductivities of the white matter and grey matter for all samples. Sample 1 to sample 6 refer to the dipole source at 10 mm, 24 mm, 38 mm, 52 mm, 66 mm and 80 mm depth. Each column indicates the average value of 6 trials of data measurement and red color error bars give the real data range dispersed from the average value.

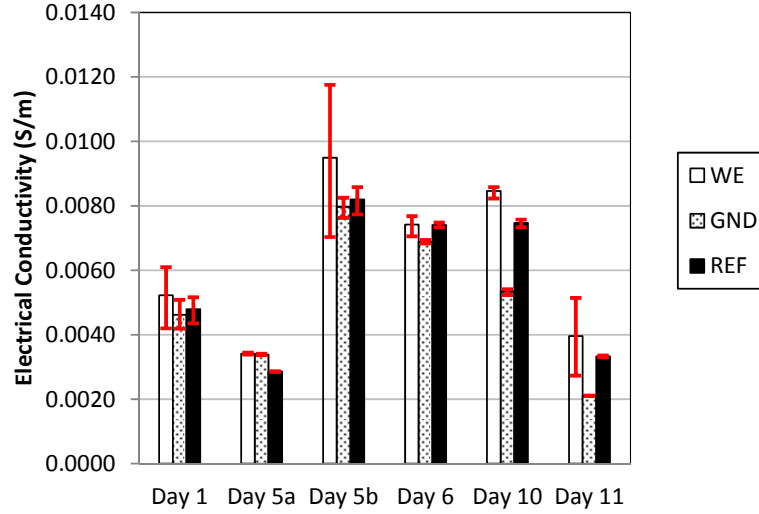


Figure 22: Prolonged test results of the electrical conductivities of the skull compartment at three electrode sites namely working electrode (WE), ground electrode (GND) and reference electrode (REF). Each column indicates the average value of 5 trials of data measurement and red color error bars give the real data range dispersed from the average value.

The dipolar source was created using a coax cable, dimensions of which were shown in Figure 23(b). The dipole source was embedded in the model at various depths as shown in Figure 23(c). One end of the coax cable was normal to the top surface while the other end was connected to the Agilent 33250A waveform generator (Agilent Technologies, Inc., Santa Clara, CA) to generate a 10 Hz continuous sinusoidal waveform with different amplitudes (5 V, 4 V, 3 V, 2 V, 1 V, 750 mV, 500 mV, 250 mV, 100 mV, 50 mV and 20 mV peak-to-peak).

The sinusoidal waveform was played for 35 seconds and its responsive surface potential signals were transmitted to ANT amplifier (ANT Neuro, Netherlands) via a working electrode placed on top surface of the model directly above the dipole source. The continuously acquired signals (sampling frequency 250 Hz)

were displayed and stored in ASA™ software (ANT Neuro, Netherlands) for further analysis (refer to Figure 23(a)).

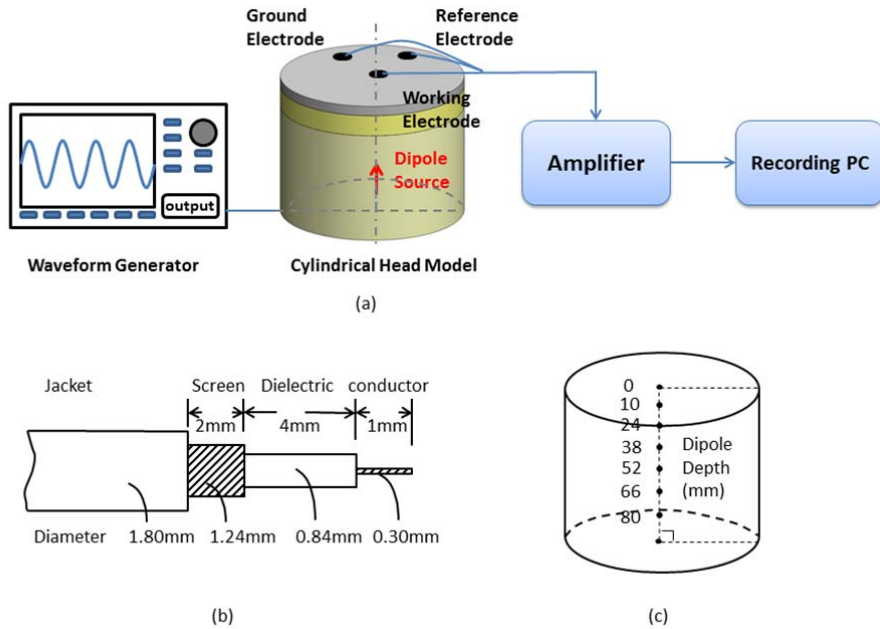


Figure 23: (a) Experiment setup, (b) dimensions of the coax cable, conductor and screen are used to generate the dipole source, and (c) configuration of the dipole position.

6.2.2 Signal processing

Considering that a short time was required for the output signal to stabilize during the experiment, a segment of data starting from 5 second and ending at 30 second were selected for Signal-to-Noise Ratio (SNR) analysis. Raw data were firstly analyzed in asa™ software by using the Fast Fourier Transform (FFT) function at 1 Hz resolution. In order not to weaken the power, filtering was not applied before executing FFT function, even notch filtering. Afterwards, the power spectrum data were imported to MATLAB R2012a

(The MathWorks Inc., Natick, Massachusetts, USA) for subsequent calculations. The power spectrum frequency was ranging from 0 Hz to 124 Hz. To find the SNRdB values, power spectrum at 0 Hz, 1 Hz and 49-51 Hz representing respectively direct current noise, consistent system noise of the acquisition equipment and power line noise were excluded from total power spectrum of noise. The SNRdB was then calculated from Equations (6.1), (6.2) and (6.3).

$$SNRdB = 10 \log_{10} \left(\frac{P_{signal}}{P_{noise}} \right) \quad (6.1)$$

$$P_{signal} = P_9 + P_{10} + P_{11} \quad (6.2)$$

$$P_{noise} = \sum_{i=0}^{124} P_i - P_{signal} - (P_0 + P_1 + P_{49} + P_{50} + P_{51}) \quad (6.3)$$

where P_i was the power at certain frequency, e.g. P_{10} was the power at 10 Hz. In general, the signal-to-noise ratio compares the level of a desired signal to the level of background noise. In this study, a threshold value of 4 dB was defined to differentiate a good signal from a bad signal. Once the signal was shown good with SNRdB above 4 dB, magnitude of the signal was calculated by the square root of P_{signal} .

6.2.3 Simulation

In addition, prior to the experiment performed, simulation was carried out in order to validate that the geometry and material properties of the head model were appropriate to use for experiment. The simulation was implemented using the electric current module in COMSOL Multiphysics® 4.4 software (Comsol Inc., Burlington, MA USA). In the simulation design, three cylinders were stacked together. The thickness and electrical property of each cylinder were consistent with those used in the experiment and all three layers were assumed to be purely conductive. Within the cylinders, volumes occupied by the inserted coax cable were removed. Areas in contact with the conductor of the cable were set to have a fixed electric potential of 5 V, areas in contact with cable screen were set to be grounded and the remaining areas were set to be insulated. The electric potential distribution at steady-state was calculated and the electric potentials of two points were sampled, one at the center of the top surface and the other one at the same surface, 41 mm away in the radial direction from the first point. Potentials of these two points were respectively taken from readings at the working and reference electrodes. The potential difference between them was taken as the desired EEG peak value.

In the simulation, depth of the inserted coax cable was altered according to the experiment design. The EEG peak values measured at different insertion depths were compared with the surface potential data acquired in the experiment. Since the simulation results and experiment results were not directly comparable, both of them were processed with unity-based normalization by Equation (6.4) and thereafter the linear correlation coefficient r value was calculated by Equation (6.5).

$$X' = \frac{X - X_{min}}{X_{max} - X_{min}} \quad (6.4)$$

$$r = \frac{n \sum(xy) - \sum x \sum y}{\left[\sqrt{n \sum(x^2) - (\sum x)^2} \right] \left[\sqrt{n \sum(y^2) - (\sum y)^2} \right]} \quad (6.5)$$

6.3 Results and Discussion

6.3.1 Comparison between experiment and simulation results

Figure 24 shows the comparison between the simulation and experiment results. The correlation coefficient r is found to be 0.9824, which indicates the two graphs are highly correlated. In other words, the experiment results are well conformed to the simulation results at the input signal of 5 V. Thus, the experiment design and selected material properties have been validated good to use for the rest of the experiment by altering the input signal amplitude.

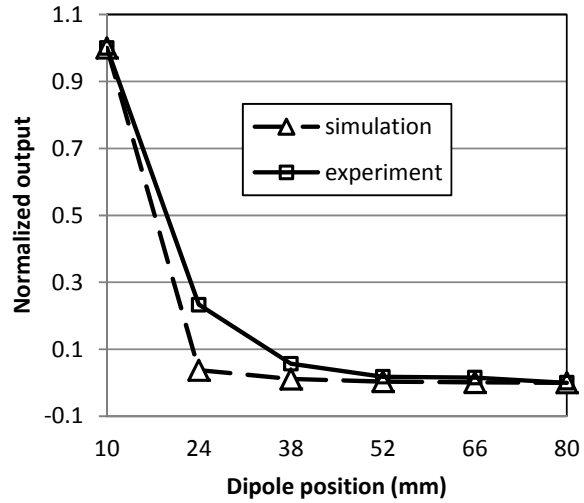


Figure 24: Comparison of experiment and simulation results, dipole source signal at 5 V.

Simulation is an ideal case where no environmental and instrumental noise is considered. Super clean signal is always calculated via simulation process. However, simulation results are useless in the real scenario where deep dipole source activity may not be observed from EEG recordings due to the significant noise incurred when the input signal becomes very weak. Thus, experiment studies have been carried out.

6.3.2 Overall experiment results

As shown in Figure 25, for the dipole source at 80 mm depth in the model, a clear surface potential waveform has been observed only when the dipole strength being equivalent to or greater than 3 V. When the dipole source is elevated to the depth of 66 mm, good output signal waveform has been observed with the dipole strength being equivalent to or greater than 500 mV. When the dipole source is embedded shallower than 24 mm, the dipole

strength can be reduced to be as low as 250 mV for those output signals being clearly observed. When the dipole source was embedded just below skull compartment at 10mm depth, the dipole strength can be reduced to be extremely low at 20 mV for generating clearly observable surface potential waveform.

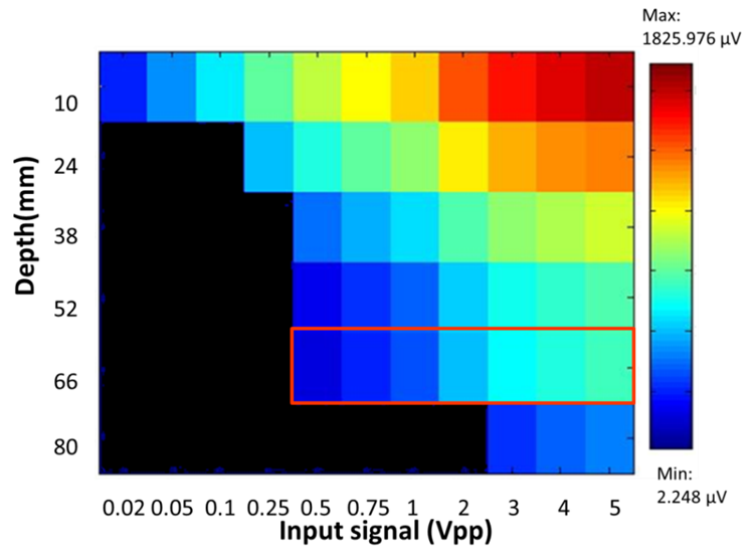


Figure 25: Colored region shows output signal amplitudes (μV) with $\text{SNR}_{\text{dB}} > 4$ dB recorded at dipole strength of 0.02, 0.05, 0.1, 0.25, 0.5, 0.75, 1, 2, 3, 4 and 5 V peak-to-peak, at dipole depth of 10, 24, 38, 52, 66 and 80 mm. Black region indicates bad signals.

Constant voltage source of 250 – 500 mV has been examined to generate dipole source of approximately 56 nA.m which is consistent with the macroscopic neural activity (Steinsträter, et al., 2010). Neuronal activities at 66 mm depth in the brain are considered as subcortical neuronal activities such as those found in basal ganglia and thalamus. Therefore, brain activities in subcortical neuronal networks with large amplitudes could be clearly observed using the non-invasive scalp EEG technique.

6.3.3 Relationship between surface potential and the depth of dipole

A further examination was carried out on the relationship between the surface potential recordings and the depth of dipole source at an input signal of 500 mV. Figure 26 depicts the exponential decay of the strength of surface potential recordings, which is well conformed to the electric field distribution in a weak conductive media, where strength of the electric field decreases rapidly with the increase of the distance from a small charged object, i.e. the dipole source in the present study. The further away from the dipole source, the less decay has been observed and that is why from 38 mm onwards, slow decay has been notified.

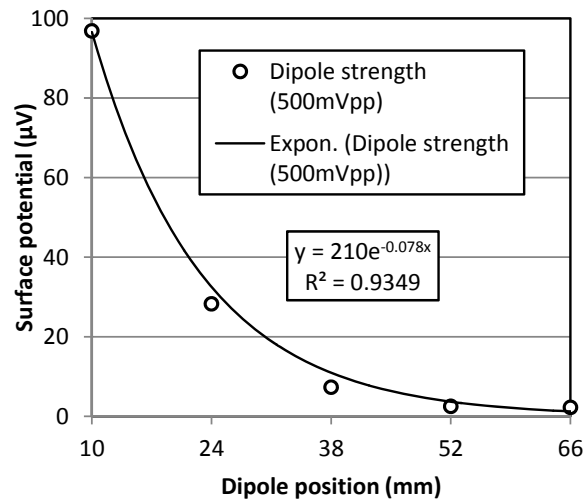


Figure 26: Surface potential amplitude decays exponentially as dipole depth increases.

6.3.4 Linearity check

Lastly when the dipole source is embedded at the depth of 66 mm, there is a relationship between the dipole strength and the surface potential recordings. A clear linear relationship has been observed (refer to Figure 27) and evidenced by the linear curve fitting ($R^2 = 0.9992$). This result is consistent with the linearity assumption of a volume conductor that is if the source strength is increased by a factor c , the resultant voltage is increased by the same factor c (Malmivuo & Plonsey, 1995).

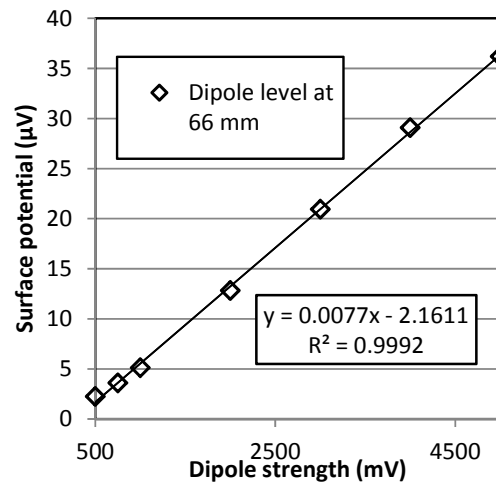


Figure 27: Linearity check of the head model.

6.4 Concluding Remarks

Deep brain activity is conventionally recorded with surgical implantation of electrodes. During the neurosurgery, brain tissue damage and the consequent side effects to patients are inevitably incurred. In order to eliminate undesired risks, we propose that deep brain activity should be measured using the non-invasive scalp electroencephalography (EEG) technique. However, the deeper the neuronal activity is located, the noisier the corresponding scalp EEG

signals are. Thus, the present study has evaluated whether deep brain activity could be observed from EEG recordings. In the experiment, a three-layer cylindrical head model was constructed to mimic a human head. A single dipole source (sine wave, 10 Hz, altering amplitudes) was embedded inside the model to simulate neuronal activity. When the dipole source was activated, surface potential was measured via electrodes attached on the top surface of the model and raw data were recorded for signal analysis. Results show that the dipole source activity positioned at 66 mm depth in the model, equivalent to the depth of deep brain structures, is clearly observed from surface potential recordings. Therefore, it is highly possible that deep brain activity could be observed from EEG recordings and deep brain activity could be measured using the non-invasive scalp EEG technique.

CHAPTER 7

Evaluation of the Performance of LORETA Method Utilized for Deep Brain Source Localization

7.1 Introduction

Low Resolution Electromagnetic Tomography (LORETA) method is widely applied in electroencephalography (EEG) source localization studies to correctly localize cortical neuronal activity in the brain. Though spatial resolution of LORETA solutions is low, the location is still acceptable by researchers in neuroscience area. However, it is unclear whether LORETA method is applicable to deep brain activities such as those found in the basal ganglia and thalamus. Those deep brain activities are considerable in neurophysiological studies for brain disease monitoring like Alzheimer's disease and Parkinson's disease. Therefore, considering the importance of deep brain activities, the present study aims to evaluate the performance of LORETA method through localization of cortical and deep brain sources.

Source localization from surface recorded electrical brain activities provides a non-invasive and easy-to-apply technique to both research and clinical settings in neurophysiological studies. The technique is to determine the position and strength of brain sources associated with surface recorded electrical potentials such as scalp electroencephalography (EEG).

LORETA algorithm is widely applied in EEG source localization studies to correctly determine the position and strength of brain sources because its spatial resolution has been demonstrated in as excellent as mm level. The

solution space was restricted to cortical grey matter and hippocampus, 7mm spatial resolution was produced. (Pascual-Marqui,1999; Pascual-Marqui, 2002). However, there is constraint of this algorithm. The solution space is restricted to cortical grey matter and hippocampus located under the cerebral cortex. In practice, deep brain activities such as those found in thalamus are more considerable for the brain disease monitoring, i.e. Parkinson's disease. If the deep brain source can be localized with this risk free technique, the invasive way such as subdural and epidural electrode recordings would be abandoned. The effect in both research and clinical settings would be great. Given the important role of deep brain activities, it is worth exploring the performance of LORETA through deep brain source localization studies.

LORETA algorithm directly computes a current distribution throughout the full brain volume. The method assumes that neighboring neurons are simultaneously and synchronously activated. In view of physiological consideration the computational task is to select the smoothest of all possible three-dimensional (3D) current distributions, a task that is a common procedure in generalized signal processing.

7.2 Materials and Methods

7.2.1 Construction of the physical head model

In this research study, a three-layer physical head model was constructed for the evaluation of LORETA method applied in deep brain activity localizations. The physical head model was composed of three layers namely the brain, skull and scalp and each layer was homogeneous and isotropic. We have previously introduced one realistic head phantom in Chapter 5. That head phantom

preserved only the cerebral hemisphere and excluded those brain structures located at subcortical regions such as the brain stem. Further, the skull and scalp layers in that head phantom formed only part of a head, similar to a cap. In contrast, the physical head model introduced here was a complete shaped model including deep brain structures.

Construction of the physical head model was realized with four procedures namely computer-aided design, rapid prototyping, casting and injection molding. Fabrication method for the skull, scalp and brain layer would be described in sequence.

The skull compartment was the first layer produced. The three-dimensional skull shape was originally purchased from AnatomiumTM (21st Century Solutions Ltd). The skull shape was modified by smoothening its surface and removing the hollow eye ball cavities. The skull aluminium mold was casted based on the treated skull surface information. Talking about the manufacturing process, the skull layer was formed via injection molding. Two molds were included in this process. One was the aforementioned skull aluminium mold and the other one was the brain master pattern which would be introduced in next paragraph. The first step of the manufacturing process was to assemble the two molds for the subsequent injection molding process. The electrically conductive silicone rubber was the ingredient to make the skull layer. The silicone rubber material was pre-processed in a vacuum chamber to ensure air bubbles being removed. The degassed silicone rubber material was then injected into the molding cavity. After that, the material and molds were placed in the oven to expedite the curing process. Once the skull

layer was fully cured, the two molds were dissembled and the final skull layer was taken out for the scalp and brain layer making.

The 3D brain model was again originally purchased from Anatomium™ (21st Century Solutions Ltd). The 3D brain model contained complete information of a real human brain. It included the cerebrum, cerebellum and brain stem structures. To make the fabrication process practical, volumetric size of the brain stem structure was enlarged to have a smooth transition and connection to the upper cerebral hemisphere (See Figure 28 (a)). The complicated cortical geometries such as sulci and gyri were preserved. As mentioned earlier, two molds were assembled to fabricate the skull layer. One of them was the brain master pattern. The 3D brain model introduced in this paragraph was used to produce this brain master pattern through rapid prototyping (RP) method.

The scalp layer was the second layer produced. It was composed of 40 layers of solidified latex rubber with a thickness of 5 mm. The scalp layer was coated with liquid latex rubber material doped with sodium chloride (NaCl) to achieve the desired electrical conductivity. Each of the 40 layers was slowly coated on the skull to make sure the latex rubber material made full coverage on the skull. After each coat, the skull layer was placed in the oven (temperature at 100 °C). This temperature level could expedite the solidifying process of the latex rubber material. However, this temperature level already exceeded the melting temperature of the gelatin material. That is why the brain layer was the last layer produced in this research study.

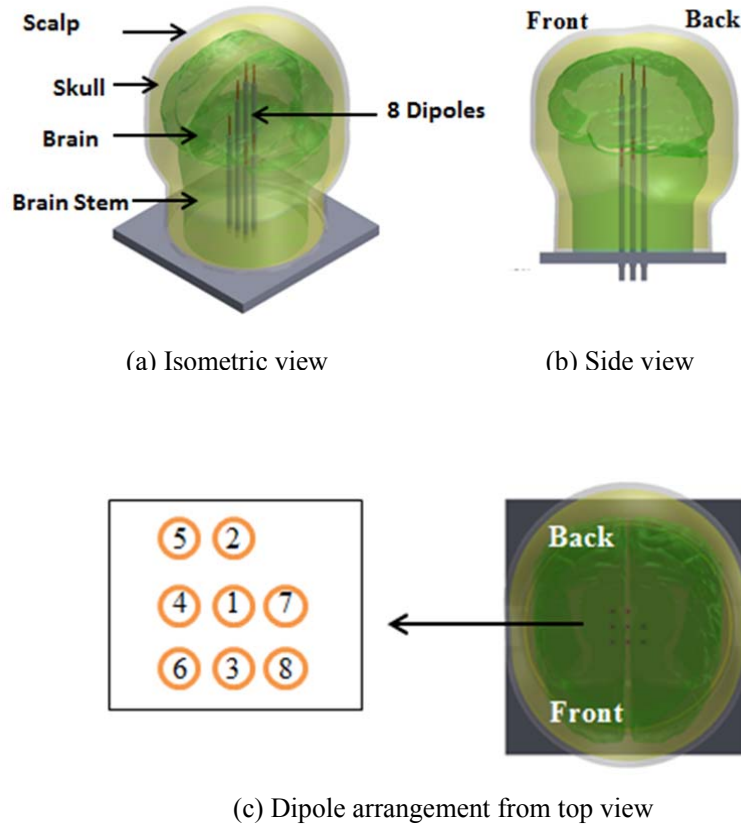


Figure 28: Three-dimensional display of the physical head model with dipoles embedded inside the brain, (a) isometric view, (b) side view, and (c) dipole arrangement from top view.

The scalp layer was made by injection of the liquid gelatin-NaCl material into the skull cavity. The whole head model was stored in the refrigerator overnight before use. Before the liquid gelatin material solidified, 8 dipoles were inserted in the brain compartment with a dipole support structure. The 8 dipoles were located at 8 different depths in the brain, with dipole D1 located on top and D8 located at bottom. Signal of the dipole was a sinusoidal waveform (10 Hz, 5 V peak-to-peak) generated by the Agilent 33250A waveform generator (Agilent Technologies, Inc., Santa Clara, CA). The frequency was chosen according to that of the brain alpha wave. The voltage

level was chosen to reproduce realistic EEG signals in μV range. The dipole source was made of coax cable with configuration consistent throughout the whole thesis.

7.2.2 Electrical property of the head model

Electrical conductivities of the brain, skull and scalp layer in this particular study were 0.379 ± 0.013 S/m, 0.0195 ± 0.0029 S/m and 0.327 ± 0.012 S/m respectively. Materials selected to construct the brain remained unchanged compared to my earlier research studies. However, materials selected to construct the skull and scalp layer were changed.

In order to prolong the material stability, conductive silicone rubber was chosen to make the skull layer. The skull layer was highly durable and hence could be reused to design such a physical head model for additional experiments. The general setup of electrical conductivity measurement was described in Chapter 3 section 3.2. Figure 29 showed the electrical conductivities of 4 sample pieces of the conductive silicone rubber material. Each column indicated the average conductivity value of 4 repeated trials and the error bar in red color gave the standard deviation dispersed from the average value. The averaged electrical conductivity ranged from 0.0166 to 0.0245 S/m. The range was acceptable since in reality the human skull has a non-uniform electrical conductivity distribution with lateral parts less conductive than top parts of the skull (Baillet, et al., 1997).

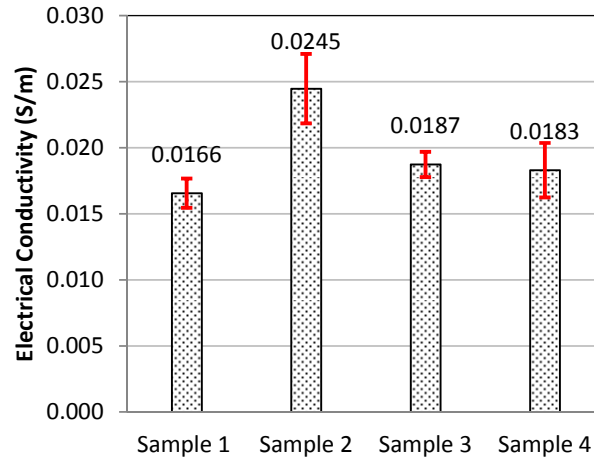


Figure 29: Electrical conductivity of 4 samples of skull material. Each column indicated the average conductivity value of 4 repeated trials and the error bar in red color gave the standard deviation dispersed from the average value.

The scalp layer was made of liquid latex material. The composition of the scalp layer included the pure liquid latex rubber (80.5 %), distilled water (16.1 %) and NaCl (3.4 %), all in weight percentage. The electrical conductivity of the scalp layer was tested on different dates. It was shown (see Figure 30) that only on day 6 the value dropped significantly. Each column indicated the average conductivity value of 18 repeated trials and the error bar in red color gave the standard deviation dispersed from the average value.

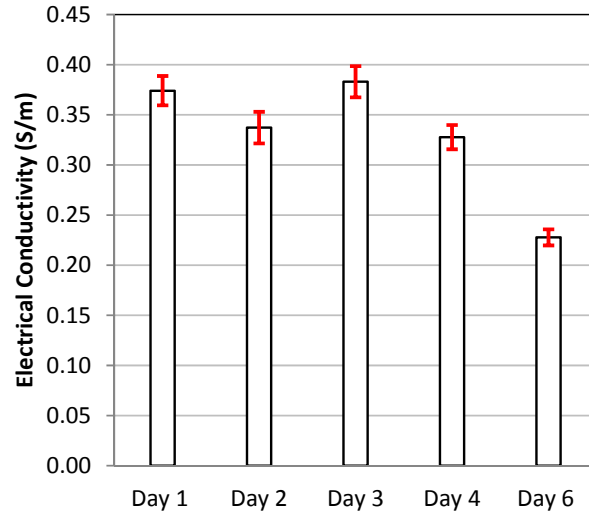


Figure 30: Prolonged electrical conductivity test of the scalp layer. Each column indicated the average conductivity value of 18 repeated trials and the error bar in red color gave the standard deviation dispersed from the average value.

7.2.3 EEG acquisition and source localization

The scalp EEG data were recorded with a WaveGuard 64-channel EEG cap and the ANT EEG amplifier (Advanced Neuro Technology, Enschede, Netherlands). In this research study, the physical head model was the testing subject. Figure 31 described the experiment setup of this study. In the experiment design, the head model was mounted and secured on an acrylic plate. Inside the head model, the pre-embedded dipoles were generating sinusoidal waveforms for 60 seconds using Agilent 33250A waveform generator (Agilent Technologies, Inc., Santa Clara, CA) and the underlying dipole activities were simultaneously displayed and saved by the EEG recording unit.

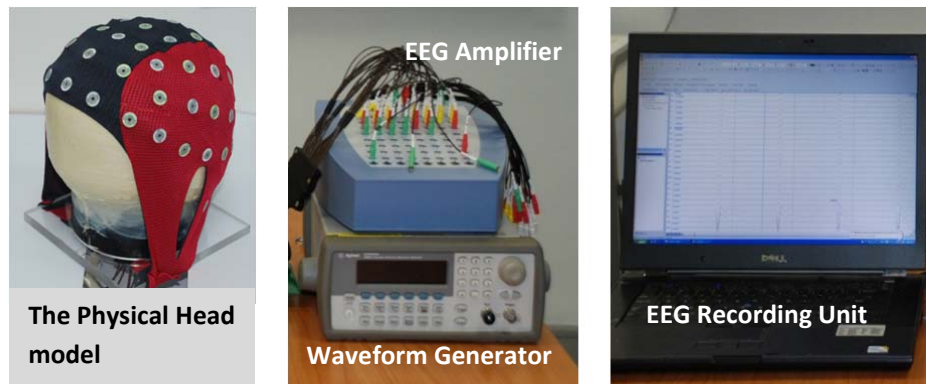


Figure 31: Experiment setup of the EEG measurement on the physical head model.

Setting up the experiment involved the injection of EEG electro-gel (Electro-gel, Electro-Cap, International, Inc., Eaton, OH) at each electrode cup. The electro-gel ensured good electric conductance between the electrode cup and the underneath scalp. The input impedance values of all channels were checked no larger than 2 k Ω throughout the whole recording session. The electrode sites of EEG measurement were in accordance with the extended international 10-20 electrode placement system (Jurcak, et al., 2007). All channels were referenced to the common average and grounded with channel AFz. The scalp EEG data were sampled at 250 Hz and were recorded and real-time displayed using asalab™ EEG acquisition software. Collected data were off-line examined and processed using asa™ signal analysis software.

Source localization was realized by using LORETA algorithm. The EEG inverse calculation was performed in sLORETA software (version 2008-11-04). The EEG data imported into this software were pre-processed with the following steps. Firstly, the raw data were band pass filtered (1 – 30 Hz) to

remove direct-current (DC) noise and unwanted high frequency noise. The original length of the data was 60 seconds. The second step was to select 25 second continuous data to do averaging. The data were selected by looking for stabilized data on the EEG scroll displayed on the recording unit. The 25 second continuous data were averaged to 1 second data. Lastly, the average data were baseline corrected.

7.3 Results and Discussion

7.3.1 EEG results

The two-dimensional (2D) displays of the EEG waveforms at each electrode site were depicted in Figure 32. This result was generated by the dipole source D1 which was located in the cortical region. Waveforms at each electrode site were sinusoidal except for some electrode sites such as C5, C6 and FT7. Signals at those electrode sides contained noisy information even though they were pre-filtered. Nonetheless, the result was acceptable as most waveforms were sinusoidal in accordance with the dipole signal information.



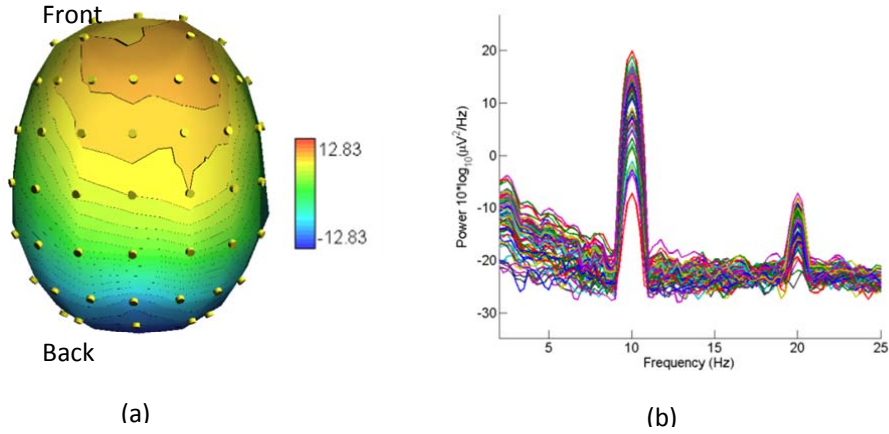


Figure 33: (a) Scalp potential map (color bar unit: μV) and (b) EEG power spectrum of dipole source D1.

In the head model design, dipole sources D1, D2 and D3 were located in the cortical region and the rest were located in the subcortical region. During EEG measurement, the dipole source signal was initially set at 2 V, 3 V, 4 V and 5 V. EEG measurements were performed for each setting. Eventually 5 V was chosen to be the final dipole source signal amplitude according to the criterion described as follows. The EEG signals generated by the cortical dipole source D1, D2 or D3 should have amplitude at tens of μV , corresponding to the amplitude of realistic EEGs.

The following EEG measurement results (see Figure 34) showed the pair of scalp potential maps and power spectra of dipole source D2 – D8. The EEG power spectra for the remaining dipoles D2 – D8 all had a significant peak at frequency of 10 Hz. The EEG power did not attenuate much when the dipole was located deeper and deeper in the physical head model. This was feasible since the EEG signals were captured by a 3D display of 62 recording electrodes. There were always some electrodes closer to the dipole location.

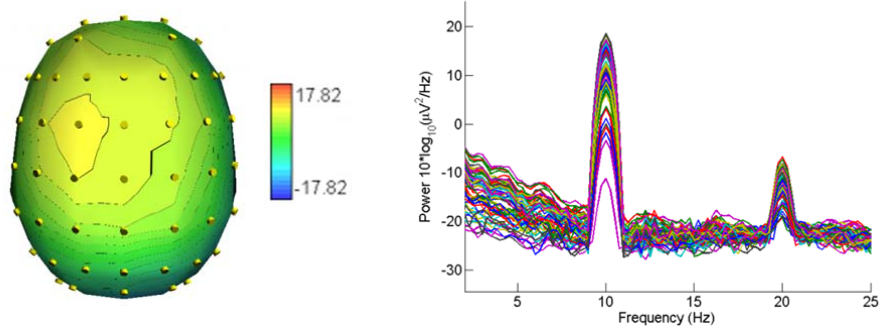
The result was different from that was explained in Chapter 6 where the surface potential recordings attenuated exponentially. The difference arose from the electrode design. In chapter 6, a single working electrode was used to record surface potentials. As the dipole was placed deeper in the cylindrical model, the distance between the working electrode and the dipole was increased. As a result, surface potential recorded by the working electrode attenuated accordingly.

It was worth noting that the EEG power generated by D7 or D8 attenuated to approximately 15 dB. This result was significant. It further confirmed the results shown in Chapter 6 that deep dipole source activities could be observed through the analysis of scalp EEG recordings.

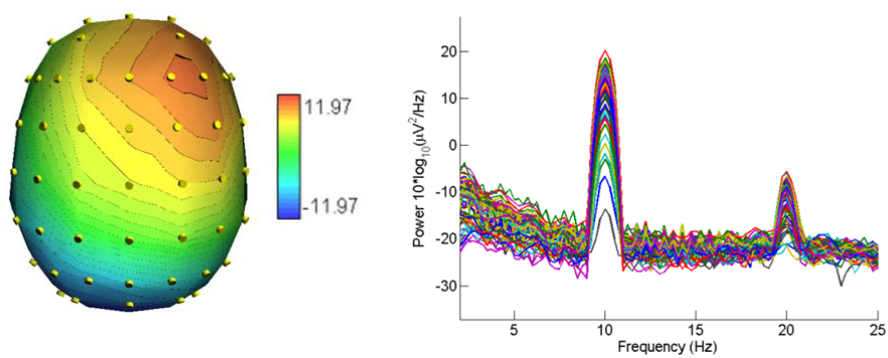
In addition, the scalp potential was concentrated at different electrode locations for different dipole sources. These results together with the scalp potential amplitudes at this electrode site were tabulated as follows (see Table 4). Referring to all dipoles, it was found that the scalp potential was concentrated on the frontal and central region.

Table 4 Electrode location and the scalp potential amplitude at this electrode site for different dipoles.

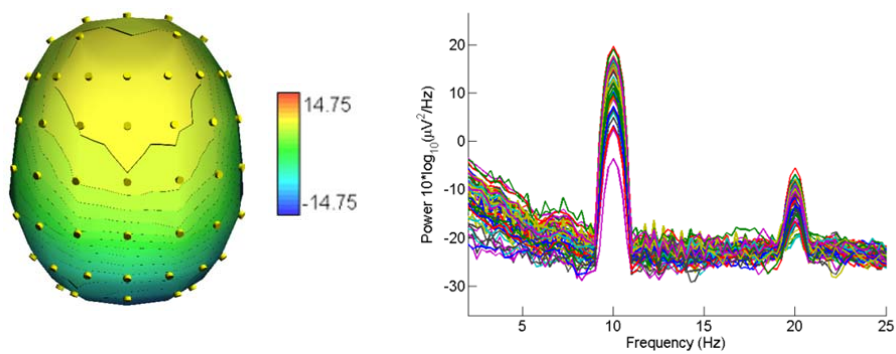
Dipole	D1	D2	D3	D4	D5	D6	D7	D8
Amplitude	9.52	10.04	10.21	8.30	7.16	8.12	5.93	5.59
(μV)								
Electrode	F2	FC1	F2	Fz	FC4	FPz	C1	FP1
Location								



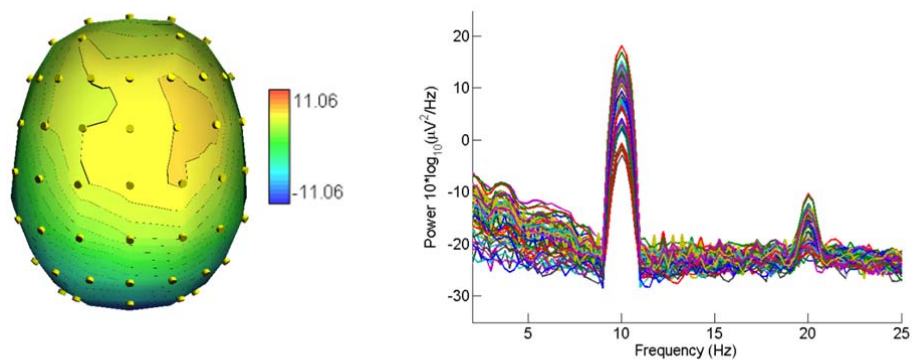
(a) D2



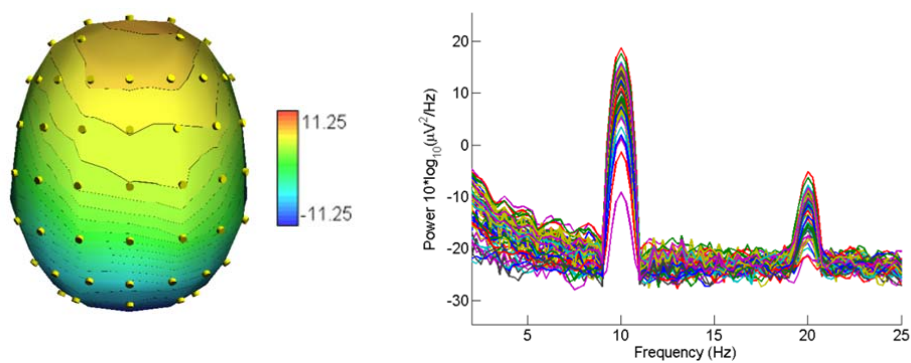
(b) D3



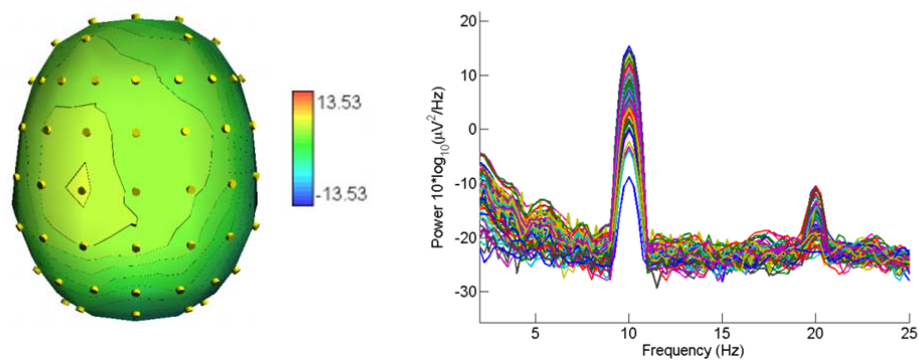
(c) D4



(d) D5



(e) D6



(f) D7

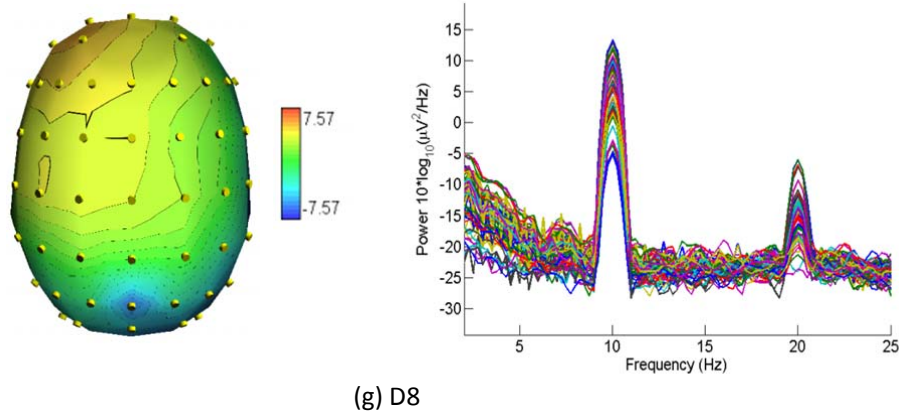


Figure 34: Scalp potential maps (all color bar units: μV) and EEG power spectra of dipole source (a) D2, (b) D3, (c) D4, (d) D5, (e) D6, (f) D7 and (g) D8.

7.3.2 Source localization results

Dipole locations were calculated by sLORETA software. Testing the accuracy of sLORETA method was evaluated in this research. The location given by the software was in Talairach space. The Talairach coordinate system specifies locations relative to their distance from the anterior commissure (AC). The AC is a small but easy to spot region, making it an ideal origin for the coordinate system. Each location is described by three numbers, each describing the distance in millimeters from the AC: X is the left/right dimension, Y is the posterior/anterior dimension, and Z is the ventral/dorsal dimension. An example of the localization results was shown in Figure 35 which was the location of dipole D1 viewed in the brain atlas.

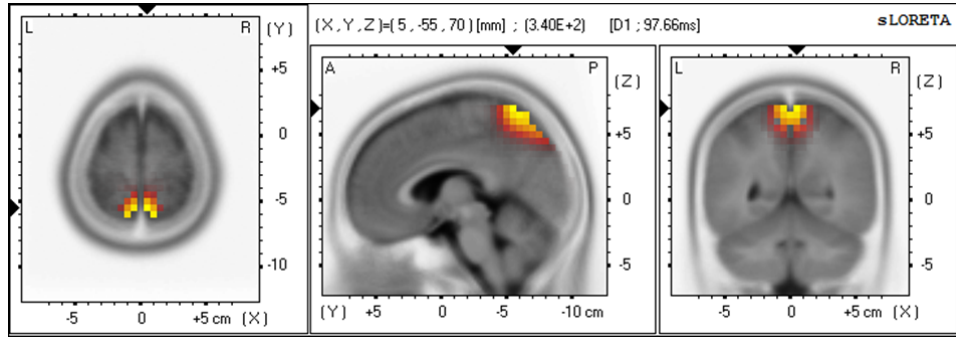


Figure 35: Source localization result of dipole D1. The hotspot region indicated location of the dipole source (X, Y, Z) in Talairach coordinate viewed in the brain atlas.

Due to brain size difference between what was designed in this research and that was given in sLORETA software, the source localization results were registered in a hemispherical head. Center of the hemisphere was taken as the origin, and the localization result (X, Y, Z) of each dipole was plotted in the hemisphere. The hemisphere was then scaled to fit into the physical brain model.

Localization error between the pre-designed dipole and the inversely calculated dipoles was shown in Figure 36. Localization error of dipoles D1 and D2 at cortex was less than 3 mm which showed very good localization accuracy. Dipole D3 though was also located at cortex, its localization error was obvious, about 17 mm. When the dipoles were located in the subcortical region (D5 and D6), the localization errors were still acceptable. When the dipoles were located even deeper in the brain (D6, D7 and D8), the localization error became significant, meaning poor localization accuracy.

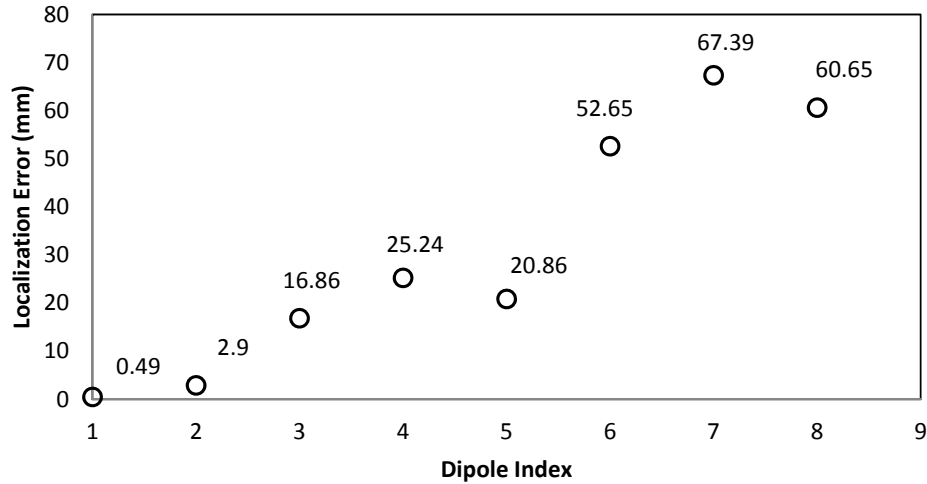


Figure 36: Localization results of the physical head model.

What could the localization accuracy tell us? The localization accuracy could tell the performance of sLORETA method for localizing cortical and deep brain activities. Observing the pre-designed dipoles in the brain anatomy (see Figure 37), dipoles D1, D2 and D3 respectively fell within somatosensory, parietal and motor cortex. In the subcortical region, dipoles D4, D5 and D6 were shown at corpus callosum, thalamus and hypothalamus respectively. When going deeper in the brain, dipoles D7 and D8 were viewed at brain stem. According to the previous result, localization error of dipole D5 (20.86 mm) was acceptable. In practice, this result indicated that Parkinson's disease caused by thalamic neuronal dysfunction could be monitored via sLORETA source localization method together with the real time EEG recordings. Further, localization accuracy of dipoles located at the subcortical region implied that subcortical brain activities in motion and memory might be also analyzed through sLORETA method.

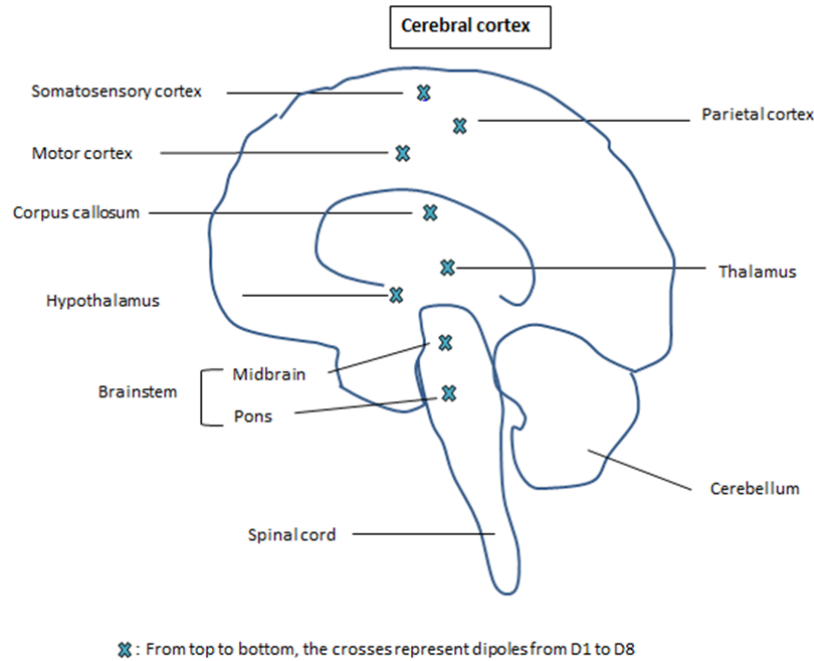


Figure 37: Schematic diagram of dipole locations in brain anatomy: D1 at somatosensory cortex, D2 at parietal cortex, D3 at motor cortex, D4 at corpus callosum, D5 at thalamus, D6 at hypothalamus, D7 and D8 at brain stem.

7.4 Concluding Remarks

This study evaluated the performance of LORETA source localization method for determining deep brain source locations. The realistic physical human head model was finally constructed for this evaluation. In the experimental design, pre-defined eight dipoles were embedded in the brain volume. Dipoles were distributed at different depths in the brain with three dipoles fell within somatosensory, parietal and motor cortex. The next three dipoles were located at subcortical structures including corpus callosum, thalamus and hypothalamus. The remaining two dipoles were located at brain stem. Sinusoidal waveforms were inputted into the dipoles and the EEG potentials recorded through surface electrodes attached on the artificial scalp were in

micro voltages. The EEG potential levels were in accordance with the realistic EEG signals. Findings showed that the localization error of LORETA method was a few millimeters for dipoles located at cortex. The location error was tens of millimeters for dipoles located at corpus callosum and thalamus in the subcortical region. However, the localization error was significant for dipoles located at hypothalamus and brain stem. In practice, these findings showed that Parkinson's disease caused by thalamic neuronal dysfunction could be monitored via sLORETA source localization method together with the real time EEG recordings. Further, localization accuracy of dipoles located at the subcortical region implied that subcortical brain activities in motion and memory might be also analyzed through sLORETA method.

CHAPTER 8

Conclusions and Recommendations for Future Work

8.1 Conclusions

This research has successfully developed the subcortical emphasized physical human head model for deep brain activity measurement via EEG technique and deep brain source localization through LORETA analysis. To our knowledge, this model is the world's first physical head model designed for subcortical and deep brain source localization studies. The novelty of this head model is attributed to the location design of its artificial neuronal sources. The artificial neuronal sources were distributed not only in the brain cortex, but also in the subcortical region and deep brain. Specifically speaking, three artificial neuronal sources were respectively distributed in corpus callosum, thalamus and hypothalamus in the subcortical region. Besides, two more artificial neuronal sources were designed to distribute in the brain stem including the midbrain and pons. The physical head model is composed of three layers, representing the human brain, skull and scalp. The electrical property of each layer is uniformly distributed. The complicated geometries of the brain surface, sulci and gyri, have been preserved for the physical model construction. The physical head model serves as an essential tool for EEG forward and inverse studies.

This research has been divided into four studies and the major findings of each study are presented as follows.

In the first study, electrically conductive electrolytes based on gelatin and NaCl were prepared and their electrical characteristics were examined. The experiment results indicate that ionic conductivity of this electrolyte is influenced by frequency, the amount of NaCl and temperature. Furthermore, the result of ionic conductivity as a function of temperature exhibited a linear relation. Different from Zhou's work (Zhou, et al., 2007), electrical characteristic study was performed both in low and high frequency ranges in this study. In addition, an empirical model that predicted ionic conductivity of gelatin-NaCl electrolyte with respect to temperature (from 25 to 50°C) and frequency (from 10 to 800 Hz) was established for the first time. This study concludes that gelatin-NaCl material is a good candidate for mimicking the brain tissue.

After the electrical characteristic study of the artificial brain material, the first version of the physical head model was constructed. This physical model was called the head phantom in order to be differentiated from the final physical human head model developed in this research. The second study evaluated the human head phantom system created for event-related potential (ERP) studies. Our approach was to compare the correlation between the experimental ERP results and the pre-defined sample ERP data. In the experiment, the dipolar sources were firstly activated with sinusoidal waveforms (10 Hz, 5 V peak-to-peak). The scalp EEG potentials were recorded for the forward matrix analysis. Based on the examination of the forward model matrix, the electrode corresponding to the underlying dipolar sources were found to conform to the pre-defined dipole locations. Furthermore, the dipolar sources were activated with the pre-defined sample ERP source waveform. Through experiment, the

ERP signals were recorded and visualized by the 2D ERP scalp map. Comparing the experimental ERP signals to the pre-defined sample ERP data, significant correlation was observed, i.e. correlation coefficient r : 0.8329 and 0.7906 ; P -value: 2.3862e-07 and 2.5602e-06. Therefore, this study has shown it is reliable to use a physical head phantom system for visual ERP studies. To some extension, the physical head model is reliable for brain activity measurement and brain source localization studies.

Having evaluated the reliability of utilizing a physical head model for EEG forward studies, this research proceeded to the third study which evaluated whether deep brain activity could be observed from EEG recordings. In the experiment, a three layer cylindrical head model was constructed to mimic a human head. A single dipole source (sine wave, 10 Hz, altering amplitudes) was embedded inside the model to simulate neuronal activity. When the dipole source was activated, surface potential was measured via electrodes attached on the top surface of the model and raw data were recorded for signal analysis. Results showed that the dipole source activity positioned at 66 mm depth in the model, equivalent to the depth of deep brain structures, was clearly observed from surface potential even with the existence of environmental and equipment noise. Therefore, this study indicated that deep brain activity could be observed from scalp EEG recordings and deep brain activity could be measured using the non-invasive scalp EEG technique.

Having showed that deep brain activity could be observed from scalp EEG recordings, the final study evaluated the performance of LORETA source localization method for determining deep brain source locations. In this study, the subcortical emphasized physical human head model was finally

constructed for this evaluation. In the experimental design, pre-defined eight dipoles were embedded in the brain volume. Dipoles were distributed at different depths in the brain with three dipoles fell within somatosensory, parietal and motor cortex. The next three dipoles were located at subcortical structures including corpus callosum, thalamus and hypothalamus. The remaining two dipoles were located at brain stem. To our knowledge, this is the first time the subcortical emphasized physical human head model was developed for subcortical and deep brain source studies. Sinusoidal waveforms were inputted into the dipoles and the EEG potentials recorded through surface electrodes attached on the artificial scalp were in micro voltages. The EEG potential levels were in accordance with the realistic EEG signals. Findings showed that the localization error of LORETA method was a few millimeters for dipoles located at cortex. The location error was tens of millimeters for dipoles located at corpus callosum and thalamus in the subcortical region. However, the localization error was significant for dipoles located at hypothalamus and brain stem. In practice, the significant findings of this study indicated that Parkinson's disease caused by thalamic neuronal dysfunction could be monitored via LORETA source localization method together with the real time EEG recordings. Further, acceptable localization accuracy of dipoles located at the subcortical region implied that subcortical brain activities in motion and memory might be also analyzed through LORETA method.

8.2 Recommendations for Future Work

Through evaluating the performance of LORETA source localization method, the findings have shown that the localization error was insignificant for neuronal activities located at cortex. Furthermore, the localization error was acceptable for neuronal activities located at subcortical region including corpus callosum and thalamus in deep brain structures. However, the localization error was significant for neuronal activities located at hypothalamus also in subcortical structures. The inconsistency of localization accuracy found in different deep brain structures is attributed to the coarse artificial brain design. The artificial brain in this research is homogeneous and has uniform electrical property throughout the whole brain volume. In reality, the structures in the brain are much more complicated than those designed in the physical head model. The brain is generally divided into grey matter and white matter. The superior cortex region is within grey matter while the underneath deep brain structures are located in the white matter. The electrical properties of the two matters are different. Further, different brain structures in the white matter referring to the subcortical region should have different electrical properties. In order to further evaluate the localization accuracy of LORETA method for each individual structure, development of a sophisticated inhomogeneous brain model with anisotropic electrical properties is recommended for future work. By doing so, researchers could understand in detail what would be the localization accuracy of utilizing LORETA method to determine the neuronal activity of a particular structure in the deep brain region.

Bibliography

- Akhtari, M., Bryant, H. C., Mamelak, A. N., Flynn, E. R., Heller, L., Shih, J. J., . . . Sutherling, W. W. (2002, March). Conductivities of Three-Layer Live Human Skull. *Brain Topography*, 14(3), 151-167.
- Anderer, P., Pascual-Marqui, R., Semlitsch, H., & B, S. (1998a). Electrical sources of P300 event-related brain potentials revealed by low resolution electromagnetic tomography .1. Effects of normal aging. *Neuropsychobiology* , 37: 20-27.
- Anderer, P., Pascual-Marqui, R., Semlitsch, H., & Saletu, B. (1998b). Differential effects of normal aging on sources of standard N1, target N1 and target P300 auditory event-related brain potentials revealed by low resolution electromagnetic tomography (LORETA). *Evoked Potentials-Electroencephalography and Clinical Neurophysiology*, 108:160-174.
- Attal , Y., Bhattacharjee, J., Yelnik, J., Cottureau, B., Lefevre, J., Okada, Y., . . . Baillet, S. (2009). Modelling and detecting deep brain activity with MEG and EEG. *IRBM*, 30(3), 133-138.
- Bailey, R. (n.d.). *Anatomy of the Brain*. Retrieved September 28, 2014, from Human Anatomy & Biology: <http://biology.about.com/od/humananatomybiology/a/anatomybrain.htm>
- Baillet , S., Marin, G., Le Rudullier, F., & Garnero, L. (1997). Evoked potentials from a real skull phantomhead: An experimental step to the validation of methods for solving the forward and inverse problems of brain cortical imaging . *Human Brain Mapping* .
- Baillet, S., Mosher, J., & Leahy, R. (2001). Electromagnetic brain mapping. *IEEE Signal Processing Magazine*, 18(6): 14-30.
- Barth, D., Sutherling, W., Broffman, J., & Beatty, J. (1986). Magnetic localization of a dipolar current source implanted in a sphere and a human cranium. *Electroencephalogr Clin Neurophysiol*, 63(3):260-73.
- Berger, H. (1929). Über das Elektroenkephalogramm des Menschen. *Archiv für Psychiatrie und Nervenkrankheiten*, 87:527-570.
- Boon, P., D'Hav, M., Vandekerckhove, T., Achten, E., Adam, C., Clmenceau, S., . . . De, R. J. (1997). Dipole modelling and intracranial EEG recording: correlation between dipole and ictal onset zone. *Acta Neurochir*, 139:643-652.

- Burger, H., & Milaan, J. B. (1943). Measurements of the specific resistance of the human body to direct current. *Acta Medica Scandinavica*, 114(6), 584-607.
- Cao, N. (2006). Parametric surface-source modeling and estimation with EEG. *IEEE Transactions on Biomedical Engineering*, 53:2414-24.
- Caton, R. (1875). The electric currents of the brain. *British Medical Journal*, 2:278-278.
- Collier, T. J., Kynor, D. B., Bieszczad, J., Audette, W. E., Kobylarz, E. J., & Diamon, S. (2012). Creation of a Human Head Phantom for Testing of Electroencephalography Equipment and Techniques. *IEEE Transactions on Biomedical Engineering*, 59 (9), 2628-2634.
- Collins, D., Zijdenbos, A., Kollokian, V., Sled, J., Kabani, N., Holmes, C., & Evans, A. (1998). Design and construction of a realistic digital brain. *IEEE Trans. Med. Imag.*, 17, 3:463-468.
- Cooper, R., Winter, A., Crow, H., & Walter, W. G. (1965). Comparison of subcortical, cortical and scalp activity using chronically indwelling electrodes in man. *Electroencephalography and Clinical Neurophysiology*, 18: 217-228.
- Cuffin, B., Cohen, D., Yunokuchi, K., Maniewski, R., Purcell, C., Cosgrove, G., . . . Schomer, D. (1991). Tests of EEG localization accuracy using implanted sources in the human brain. *Ann Neurol*, 29(2):132-8.
- Dauwels, J., Vialatte, F., & Cichocki, A. (2010). Diagnosis of Alzheimer's disease from EEG signals: where are we standing? *Curr Alzheimer Res*, 7(6), 487-505.
- Delorme, A., & Makeig, S. (2004). EEGLAB: an open source toolbox for analysis of single-trial EEG dynamics. *Journal of Neuroscience Methods*, 134: 9-21.
- Draper, N., & Smith, H. (1998). Applied regression analysis (wiley series in probability and statistics).
- Fuchs, M., Kastner, J., Wagner, M., Hawes, S., & Ebersole, J. (2002). A standardized boundary element method volume conductor model. *Clinical Neurophysiology*, 113, 702-12.
- Gallinat, J., Mulert, C., Bajbouj, M., Herrmann, W., Schunter, J., Senkowski, D., . . . Winterer, G. (2002). Frontal and temporal dysfunction of auditory stimulus processing in schizophrenia. *NeuroImage*, 7:110-127.

- Gedders, L., & Baker, L. (1967). The specific resistance of biological material - a compendium of data for the biomedical engineer and physiologist. *Med. Biol. Eng. Comput.*, 5(3), 271-293.
- Greenblatt, R., & Robinson, S. (1994). A simple head shape approximation for the 3 shell model. *Brain Topogr*, 6, 4:331-331.
- Hallett, M. (1990). Clinical neurophysiology of akinesia. *Rev Neurol*, 146, 585-590.
- Han, C.-X., Wang, J., Yi, G.-S., & Che, Y.-Q. (2013). Investigation of EEG abnormalities in the early stage of Parkinson's disease. *Cogn Neurodyn*, 7:351-359.
- Harris, C. M. (2013, May 10). *Scalp Anatomy*. Retrieved September 28, 2014, from Medscape: <http://emedicine.medscape.com/article/834808-overview>
- Hatta, F. e. (2009). Plasticized PVA/PVP-KOH alkaline solid polymer blend electrolyte for electrochemical cells. *Functional Material Letters*, 2(3): 121-125.
- Hirota, T., Yagyu, T., Pascual-Marqui, R., Saito, N., & Kinoshita, T. (2001). Spatial structure of brain electric fields during intermittent photic stimulation. *Neuropsychobiology*, 44: 108-112.
- Indiradevi, K., Elias, E., & Sathidevi, P. (2008). Automatic localisation of epileptic foci in long-term continuous EEG. *International Journal of Medical Engineering and Informatics*, 1(1): 134-154.
- Jurcak, V., Tsuzuki, D., & Dan, I. (2007). 10/20, 10/10, and 10/5 systems revisited: their validity as relative head-surface-based positioning systems. *Neuroimage*, 34(4):1600-11.
- Khateb, A., Alan, J. P., Christoph, M. M., Theodor, L., & Jean-Marie, A. (2002). Dynamics of brain activation during an explicit word and image recognition task: an electrophysiological study. *Brain Topography*, 14.
- Khateb, A., Michel, C., Pegna, A., Landis, T., & Annoni, J. (2000). New insights into the stroop effect: a spatiotemporal analysis of electric brain activity. *Neuroreport*, 11: 1849-1855.
- Khateb, A., Michel, C., Pegna, A., Thut, G., Landis, T., & Annoni, J. (2001). The time course of semantic category processing in the cerebral hemispheres: an electrophysiological study. *Cognitive Brain Research*, 10: 251-264.

- Khateb, A., Pegna, A. J., Michel, C. M., Landis, T., & Annoni, J. (2002). Dynamics of Brain Activation During an Explicit Word and Image Recognition Task: An Electrophysiological Study. *Brain Topography*, 14(3), 197-213.
- Kozlov, P., & Burdygina, G. (1983). The structure and properties of solid gelatin and the principles of their modification. *Polymer*, 24, 651-666.
- Krings, T., Chiappa, K., Cocchius, J., Connolly, S., & Cosgrove, G. (1999). Accuracy of EEG dipole source localization using implanted sources in the human brain. *Clinical Neurophysiology*, 110:106-114.
- Kuss, J., Wagner, S., Meyer, T., Kirsch, M., Werner, A., Schackert, G., . . . Morgenstern, U. (2011). A head phantom prototype to verify subdural electrode localization tools in epilepsy surgery. *Neuroimage*, Suppl 1:S256-62.
- Lantz, G., Michel, C., Pascual-Marqui, R., Spinelli, L., Seeck, M., Seri, S., . . . Rosen, I. (1997). Extracranial localization of intracranial interictal epileptiform activity using LORETA (low resolution electromagnetic tomography). *Electroencephalography and Clinical Neurophysiology*, 102: 414-422.
- Lazebnik, M., Madsen, E., Frank, G., & Hagness, S. (2005). Tissue-mimicking phantom materials for narrowband and ultrawideband microwave applications. *Phys Med Biol*, 50(18):4245-58.
- Leahy, R., Mosher, J., Spencer, M., Huang, M., & Lewine, J. (1998). A study of dipole localization accuracy for MEG and EEG using a human skull phantom. *Electroencephalogr Clin Neurophysiol*, 107(2):159-73.
- Lewine, J., Edgar, J., Repa, K., Paulson, K., Astur, R., & Orrison Jr, W. (1995). A physical phantom for simulating the impact of pathology on magnetic source imaging. in *Biomagnetism: Fundamental Research and Clinical Applications*, 368-372.
- Li, X., & Duc, B. (2012). Functional neuroimaging of circadian fatigue. *International Journal of Computer Applications in Technology*, 45(2/3):156-162.
- Li, Y., Tong, S., Liu, D., Gai, Y., Wang, X., Wang, J., . . . Zhu, Y. (2008). Abnormal EEG complexity in patients with schizophrenia and depression. *Clinical Neurophysiology*, 119(6), 1232-1241.
- Liu, A. K., Dale, A. M., & Belliveau, J. W. (2002). Monte Carlo simulation studies of EEG and MEG localization accuracy. *Human Brain Mapping*, 16 (1), pp. 47-6.

- Malmivuo, J. A., & Plonsey, R. (1995). Bioelectromagnetism, Chapter 11. *Oxford University Press, New York.*
- Marchal, C., Nadi, M., Tosser, A. J., Roussey, C., & Gaulard, M. L. (1989). Dielectric properties of gelatin phantoms used for simulations of biological tissues between 10 and 50 MHz. *International Journal of Hyperthermia*, 5(6), 725-732.
- Merlet, I. (2001). Dipole modeling of interictal and ictal EEG and MEG paroxysms. *Epileptic Disord*, 3:11-36.
- Miklavcic, D., Pavselj, N., & Hart, F. (2006). Electric properties of tissues. *Encyclopedia of Biomedical Engineering.*
- Mulert, C., Gallinat, J., Pascual-Marqui, R., Dorn, H., Frick, K., Schlattmann, P., . . . Winterer, G. (2001). Reduced event-related current density in the anterior cingulate cortex in schizophrenia. *Neuroimage*, 13: 589-600.
- Nadi, M., Prieur, G., & Marchal, C. (1990). Development of a gelatin water phantom used for simulation of biological tissues in the 20-110 MHz band. *IEEE*, 2099-2100.
- Nunez, P., & Srinivasan, R. (2005). Electric Fields of the Brain: The Neurophysics of EEG 2nd ed. *New York: Oxford Univ. Press.*
- Okano, Y., Ito, K., Ida, I., & Takahashi, M. (2000). The SAR evaluation method by a combination of thermographic experiments and biological tissue-equivalent phantoms. *Microwave Theory and Techniques, IEEE Transactions on*, 48(11), 2094 - 2103.
- Oosten, T., Delbeke, J., & Stegeman, D. (2000). The conductivity of the human skull: results of in vivo and in vitro measurements. *IEEE Trans. Biomed. Eng.*, 47(11), 1487-1492.
- Oosten, T., Delbeke, J., & Stegeman, D. (2000). The conductivity of the human skull: results of in vivo and in vitro measurements. *IEEE Transactions on Biomedical Engineering*, 47(11), 1487-1492.
- Pascual-Marqui, R. (1999). Review of methods for solving the EEG inverse problem. *International Journal of Bioelectromagnetism*, 1, 1:75-86.
- Pascual-Marqui, R. (2002). Standardized low resolution brain electromagnetic tomography (sLORETA):technical details. *Methods and Findings in Experimental & Clinical Pharmacology*, 24D:5-12.

- Pascual-Marqui, R., Michel, C., & Lehmann, D. (1994). Low resolution electromagnetic tomography: a new method for localizing electrical activity in the brain. *Int J Psychophysiol*, 18(1):49-65.
- Philips, H. (2006, September 04). *Introduction: The Human Brain*. Retrieved September 2014, from NewScientist:
<http://www.newscientist.com/article/dn9969-introduction-the-human-brain.html?full=true#.VCfDwvmSySp>
- Pizzagalli, D., Lehmann, D., Koenig, T., REGARD, M., & Pascual-Marqui, R. (2000). Face-elicited ERPs and affective attitude: brain electric microstate and tomography analyses. *Clinical Neurophysiology*, 111: 521-531.
- Rajendran, S., & Uma, T. (2000). Lithium ion conduction in PVC–LiBF₄ electrolytes gelled with PMMA. *Journal of Power Sources*, 88(2): 282-285.
- Rush, S., & Driscoll, D. (1968). Current distribution in the brain from surface electrodes. *Anesthesia & Analgesia*, 47(6): 717-723.
- Seeck, M., Lazeyras, F., Michel, C., Blanke, O., Gericke, C., Ives, J., . . . Landis, T. (1998). Non-invasive epileptic focus localization using EEG-triggered functional MRI and electromagnetic tomography. *Electroencephalography and Clinical Neurophysiology*, 106: 508-512.
- Shmueli, K., Thomas, D., & Ordidge, R. (2007). Design, construction and evaluation of an anthropomorphic head phantom with realistic susceptibility artifacts. *J. Magn. Reson. Imag*, 26, 1:202-207.
- Spencer, M., Leahy, R., & Mosher, J. (1996). A skull based multiple dipole phantom for EEG and MEG studies. *Biomagnetism conference*.
- Steinsträter, O., Sillekens, S., Junghoefer, M., Burger, M., & Wolters, C. (2010). Sensitivity of beamformer source analysis to deficiencies in forward modeling. *Hum Brain Mapp*, 31(12), 1907-27.
- Thomas, F. N., Andrew, F. L., Wilfred, G. v., Charles, H. H., Mark, M., & Herbert, W. (1997). EEG power correlates with subcortical metabolic activity in AIDS. *The Journal of Neuropsychiatry and Clinical Neurosciences*, 9:574-578.
- Thut, G., Hauert, C., Morand, S., Seeck, M., Landis, T., & Michel, C. (1999). Evidence for interhemispheric motor-level transfer in a simple reaction time task: an EEG study. *Experimental Brain Research*, 128: 256-261.

- Valls-Solé, J., & valldeoriola, F. (2002). Neurophysiological correlate of clinical signs in Parkinson's disease. *Clinical Neurophysiology*, 113:792-805.
- Van, L. T., Steinhausen, H., Overtom, C., Pascual-Marqui, R., Van't Klooster, B., Rothenberger, A., . . . Brandeis, D. (1998). The continuous performance test revisited with neuroelectric mapping: impaired orienting in children with attention deficits. *Behavioural Brain Research*, 94: 97-110.
- Wolters, C., Anwander, A., Tricoche, X., Weinstein, D., Koch, M., & MacLeod, R. (2006). Influence of tissue conductivity anisotropy on EEG/MEG fieldand return current computation in a realistic head model: A simulation and visualization study using high-resolution finite element modeling. *NeuroImage*, 30, 3:813-826.
- Worrell, G., Lagerlund , T., Sharbrough, F., Brinkmann, B., Busacker, N., Cicora, K., & O'Brien, T. (2000). Localization of the epileptic focus by low-resolution electromagnetic tomography in patients with a lesion demonstrated by MRI. *Brain Topogr*, 12(4):273-82.
- Zhou, Z.-z., Pockett, S., Brennan, B., Chun-huan, X., & Bold, G. (2007). Physical characteristics of simulated human brain. *Journal of Chinese Clinical Medicine*, 2(4): 231-235.